THE UNIVERSITY OF ALBERTA

LINEAR TRANSIENT GAS FLOW THROUGH POROUS MEDIA

by

© A. P. Cachero

A THESIS

SUBMITTED TO THE FACULTY OF GRADUATE STUDIES

IN PARTIAL FULFILMENT OF

THE REQUIREMENTS FOR THE DEGREE OF

MASTER OF SCIENCE IN PETROLEUM ENGINEERING

FACULTY OF ENGINEERING

DEPARTMENT OF CHEMICAL AND PETROLEUM ENGINEERING

EDMONTON, ALBERTA

SPRING, 1969

UNIVERSITY OF ALBERTA

FACULTY OF GRADUATE STUDIES

The undersigned certify that they have read, and recommend to the Faculty of Graduate Studies for acceptance, a thesis entitled "Linear Transient Gas Flow Through Porous Media", submitted by Alberto P. Cachero in partial fulfilment of the requirements for the degree of Master of Science in Petroleum Engineering.

ABSTRACT

Equipment capable of measuring unsteady-state pressure changes in cores at time intervals as close as 0.6 seconds has been designed. To test the validity of this equipment for pressure transient analysis, analogous unsteady flow processes in the form of pressure drawdown and pressure buildup were performed. Conditions of finite and infinite external boundary cases in linear systems were simulated. The transient curves were graphically illustrated and analyzed. Steady-state flow tests were also run to determine permeabilities of the core samples and possible delineation of turbulent flow regimes.

From the steady-state flow tests, damage was observed on both ends of the Berea Sandstone Core. This damage was attributed to two possibilities: namely, mechanical end effects and damage due to possible exposure to fresh water. For the Alundum core, it was possible to determine the flow rates and mean pressures where turbulent flow occurred. The curves illustrating the unsteady-state tests showed the influence of permeability variation of a linear system on pressure transients. They qualitatively affirmed some important theories and observations on pressure drawdown and pressure buildup analyses.

The experimental pressure distributions of the drawdown tests, constant inlet pressure case, were compared with numerical solutions where the Crank-Nicholson Method was used as an averaging technique for distance-derivatives. The numerical solutions were found to be generally lower than the experimental values and these deviations tended to follow a definite pattern. These discrepancies between the calculated and experimental results were subsequently explained.

ACKNOWLEDGEMENT

The writer wishes to express sincere appreciation to Dr. D. L. Flock, under whose guidance and supervision this investigation was completed, to the Alberta Research Council for its financial assistance and to the staff of the Chemical and Petroleum Engineering Shop for their assistance in the construction of the equipment.

TABLE OF CONTENTS

LIST OF TABLES

LIST OF FIGURES

LIST OF FIGURES - continued

INTRODUCTION

Transient well testing in the form of pressure drawdown and pressure buildup analyses has found extensive use in the estimation of reserves, detection of barriers or faults, general performance of oil and gas wells, and recently in analyzing well stimulation methods. Various methods for analyzing pressure buildup relationships have appeared in literature [1 - 8] and are classified according to the reservoir boundary conditions assumed in their derivations. These boundary conditions have been conveniently divided into two categories: (1) a small inner boundary (well bore) and a sufficiently large but finite outer boundary at which the pressure remains constant or where no influx of fluid occurs; and (2) an infinitely small inner boundary and infinitely large outer boundary. The external boundary refers to the drainage limit or the extent to which there is flow of fluid toward the well bore. In an infinite reservoir case the pressure at the infinite boundary is always equal to the original pressure. The reservoir with a finite boundary with no influx is surrounded by a boundary which is impermeable to fluid flow. In contrast, for the case of a finite reservoir with a constant external pressure, there is fluid flow across the boundary sufficient to maintain the pressure constant at the boundary.

From the theory of pressure buildup, the reliability of the calculated reservoir properties primarily depends upon locating the proper straight-line portion of the pressure versus logarithm of shut-in time curve. Deviations from this straight line result from the following factors:

1. physical defects in the well casing

2. phase behavior transformation of the flowing fluid
3. incomplete buildup
4. presence of some barriers or faults in the reservoir
5. existence of more than one permeability in the formations surrounding the well bore
6. non-constant rate of production prior to shut-in.

This work has as its main objective the establishment of an experimental basis and equipment for analyzing pressure transient phenomena in gas flow through a linear porous system. To attain this objective, it was necessary to perform transient flow tests and establish the validity of such tests. Therefore, unsteady-state gas flow tests were run in mounted Berea Sandstone and Alundum cores and pressures were measured at different points along the cores. Attempts were made to simulate gas flow where pressure is constant at a boundary and also where no influx occurs at a finite boundary. The pressure curves were analyzed in relation to time and permeability variations along the core.

The study was extended by solving numerically, using the Crank-Nicholson averaging technique, the pressures in the drawdown tests, constant inlet pressure case. The solutions were compared with the experimental values.

In order to determine the permeabilities of the cores and also the ranges where turbulent flow conditions exist, steady-state flow tests were performed on the same cores used in the transient flow tests.

A secondary objective of this study was to draw conclusions from both, the experimental steady-state and unsteady-state flow tests.

LITERATURE REVIEW

The review of literature reveals that very few of the published works on unsteady-state flow through porous media are experimental. Perrine [9] made use of an electrical analog to simulate and compare effects of the parameters governing pressure buildup. Landrum et al [10] established the similarity between gas equations in porous media and heat conduction equations, which enabled them to design heat conduction models simulating the flow of fluid in an unsymmetrical reservoir. The models, however, were limited to finding the relationship of well location and pressure distribution during unsteady-state depletion.

Goodknight et al [11], in their work to determine the influence of dead-end pore volume during unsteady-state flow in porous media, designed a linear core model with simulated dead-end pores, with which unsteady-state flow tests were performed. For measurement of instantaneous pressures along the model, they used transducers and recorders similar to those used in this work.

Bruce et al [12] mentioned briefly their experimental results obtained to check their numerical solutions of pressure distribution in a linear model during an unsteady-state, constant rate test. For pressure measurement ordinary pressure gauges were used. No description, however, was given on how the constant production rate of nitrogen gas was attained, which surely would pose the main problem in the experiment.

A derivation of equations applicable to problems involving unsteady-state gas flow through porous media always leads to a second order, non-linear differential equation to which no analytical solution is presently available. Approximate analytical solutions, however, have

appeared in literature [13 - 15] and found practical use in the field, but only to a limited extent. With the advent of computers, better approximations to the solutions of the same equations were developed. One of the first works published in 1953 was that of Jenkins and Aronofsky [16]. They approximated a transient solution to the diffusivity equation by introducing an effective drainage radius in the following normalized form:

$$\lambda = 1_n (r/rw) \tag{1}$$

and the differential equation then becomes

$$\frac{\partial^2 (P/Po)^2}{\partial \lambda^2} = \frac{2\phi\mu rw^2 (r/rw)^2}{KPo} \frac{\partial (p/po)}{\partial t} \tag{2}$$

From the finite-difference form of the above equation, pressure changes were ultimately calculated in a step-by-step procedure. For the constant production rate case and for both the infinite and finite closed-outer boundary cases, they related well bore pressure changes and also drainage radius with time. Particularly related to this work were their solutions of the case where pressure at the well bore was held constant and the outer boundary was assumed to be impervious. They presented their results in the form of pressure distribution within the reservoir, with time as parameter, for the case where the well bore pressure was suddenly dropped to a constant value. It was shown that before the pressure at the outer radius of the reservoir had changed, the curves for different radial positions were parallel. Then as the outer region of the reservoir was drained all of the curves converged to the value of the well bore pressure.

Bruce, Peaceman and Rachford [12] also solved the diffusivity

equation which was normalized to dimensionless form as

$$\frac{\partial^2 \underline{P}^2}{\partial \underline{X}^2} = \frac{\partial \underline{P}}{\partial \underline{t}} \qquad (3)$$

Appropriate initial and boundary conditions corresponding to constant pressure and no influx at the boundaries were fixed to solve the case of a constant production rate. Solutions were presented as pressure distribution for different times at constant production rates. From the results of their linear model two significant conclusions particularly related to this work were drawn, namely:

1. For the no-cross flow boundary case, once the pressure transient had reached the external boundary, the rate of pressure decline at every point of the system was uniform.
2. The pressure gradient was a maximum near the outlet and decreased towards the inlet. Consequently, as the rate of production decreased, the pressure distribution along the model tended to be more linear. For the no-cross flow case, the pressure gradient at the boundary approached zero.

In all of the above and other similar studies, two of the basic assumptions made were a constant permeability K and viscous flow. Upon publication and verification of the Klinkenberg permeability concept for gases, Collins and Crawford [17] tried to improve calculations on unsteady-state gas flow by correcting for the Klinkenberg effect. This they accomplished by using the Klinkenberg permeability expressed as

$$K = K_{abs} \ (1+b/Pm) \qquad (4)$$

instead of a constant permeability.

Jones [18] tried to improve unsteady-state radial gas flow calculations by using the quadratic flow form proposed by Green and Duwez [19], expressible as

$$\partial P/\partial r = \mu q/KA + \rho\beta(q/A)^{(2)} \qquad (5)$$

where β is an empirical constant. In showing the applicability of the above equation, especially where flow becomes turbulent, Jones compared his results to those of Aronofsky and Jenkins [20] and Bruce et al [12].

MATHEMATICAL MODEL

The mathematical model formulated consists of the simultaneous solution of the equations of:

1. continuity
2. state
3. motion of flow

For a one-dimensional model in which only single-phase gas flow occurs, the above equations may be written as follows:

continuity $$\partial(\rho q)/\partial x + \phi \partial \rho/\partial t = 0 \qquad (6)$$

state $$\rho = MP/ZRT \qquad (7)$$

motion $$q = (-K\partial P)/(\mu \partial x) \qquad (8)$$

Equation (7) assumes that the gas obeys the modified gas law and Equation (8), that gas flow may be described by Darcy's law. Equation (8) as written holds only for gases in the viscous flow regime, under conditions of negligible slippage effects. The "slip" phenomenon in gas flow is the condition whereby the gas layer immediately adjacent to the walls of the flow channel also moves in the direction of flow. Investigators [21,22] have shown that slippage is directly proportional to the mean free path of the gas molecules which in turn is inversely related to the mean pressure. In an actual gas flow problem where slippage is considered, the permeability K in Equation (8) is the apparent permeability K_{app} which is the actual permeability that the porous medium has to a certain fluid at certain conditions of flow. Neglecting slippage implies that the permeability in the equation is absolute. As such, permeability is a function of the porous medium only. The relationship of these two permeabilities has been the subject

of extensive studies. The absolute permeability as used in Equation (8) may be evaluated by extrapolation of the Klinkenberg plot.

The above equations with initial and boundary conditions appropriate to the infinite boundary case were used to describe mathematically the drawdown tests performed on the physical model. The complete set of assumptions applicable to the mathematical and laboratory models are as follows:

1. flow is horizontal and linear
2. the only flowing phase is gas of constant composition, obeying the ideal gas law
3. gravitational forces are negligible
4. the process is isothermal
5. the flow obeys Darcy's law
6. compressibility and viscosity of nitrogen are assumed constant
7. permeability to gas is constant at each section of the core and independent of pressure

The substitution of Equations (7) and (8) into (6) gives the following non-linear partial differential equation:

$$\frac{\partial}{\partial x}\left[\frac{K\partial(P^2)}{\partial x}\right] = \phi\mu\left[\frac{1}{P}\right]\frac{\partial(P^2)}{\partial t} \qquad (9)$$

Approximate analytical solutions to the above equation have been derived [14,15] after assuming a constant value of pressure in the coefficient of the time derivative term, thus linearizing the equation. However, the use of these solutions poses the problem of what average pressure to assume.

In this work Equation (9) was solved numerically. Replacing

it with finite differences and using the Crank-Nicholson method for averaging technique, the following equation is obtained:

$$\left[K_{i-\frac{1}{2}} (Y_{i-1} - Y_i) + K_{i+\frac{1}{2}} (Y_{i+1} - Y_i)\right]^{(n+1)} + \left[K_{i-\frac{1}{2}} (Y_{i-1} - Y_i) + K_{i+\frac{1}{2}} (Y_{i+1} - Y_i)\right]^{(n)} = M_i \left(Y_i^{(n+1)} - Y_i(n)\right) \qquad (10)$$

where

$$Y = p^2$$

$$M_i = \frac{2\emptyset\mu(\Delta X)^2}{\Delta t \quad P_i}$$

A problem similar to that of analytical solutions also exists in the evaluation of M_i. This is so because, for a better approximation of M_i, P_i must be the average pressure between time t_n and t_{n+1}. But the pressure at t_{n+1} is unknown. Therefore, the following iterative procedure was used:

$$M_{i,n}^{(r+1)} = M_{i,n}^{(r)} + \frac{M_{i,n}^{(r)} - Mi,n^{(r-1)}}{2} \qquad (11)$$

where r is the number of iterations. Initially $M_{i,n}^{(1)} = M_{i,n-1}$ may be used.

Equation (10) was applied to each segment of the model for any time, resulting in a system of equations which were easily solved by ordinary methods. The coefficient matrix is tri-diagonal and diagonally dominant. With equation (11), convergence was easily obtained (at most four iterations) for the error of one percent set in the program. Details of the complete program are given in Appendix III.

FLUID AND ROCK PROPERTIES

Although it was not absolutely necessary that compressibility and viscosity of the fluid be constant in order to solve equations (6), (7), (8) and (9), the analysis of the pressure transient with respect to the rock properties would certainly be much simpler if these fluid properties were fairly constant.

Compressibility of nitrogen at 78° was plotted against pressure up to 32 atmospheres as shown in Figure 1A. Values were interpolated from experimental data [23], for temperatures at 62°F and 80°F. From the relationship two straight-line portions are discernible, one from 0 to 18 atmospheres and the other from 18 to 60 atmospheres. The change of compressibility from 0 to 18 atmospheres was only 0.2%. Similarly, the relationship of viscosity of nitrogen against pressure was a straight line up to 32 atmospheres [24], and the change of viscosity in the range of 0 to 18 atmospheres was about 1.3%. As the tests in this work were conducted with pressures only as high as 11 atmospheres, the use of constant compressibility and viscosity were therefore assumed reasonable.

As methods for finding porosities of long mounted cores (i.e. the saturation technique) have the possibility of damaging the cores, their porosities were determined from small cylindrical samples at different points of a separate core but of the same material as the mounted cores. Using the Boyle's Porosimeter, the following were established as porosities of three samples from the Berea Sandstone: 18.18%, 17.50% and 18.10%. Porosities of two samples from the Alundum Core were 28.91% and 28.95%.

Permeability variation along each core was determined from steady-state flow tests. For a real gas flowing through a linear

homogeneous core at a steady-state condition, the integrated form of Darcy's Law shows that the relationship of pressure-squared against distance along the core was linear. A non-linear graph may indicate heterogeneity of the core or non-viscous conditions of flow. In the experiment it was established that the Berea core was homogeneous, and non-linearity of the steady-state flow curves was due to damage at both ends of the core. Average permeabilities were obtained for the different sections of the core where the steady-state flow curves were linear.

EXPERIMENTAL EQUIPMENT

Figure 1 is a schematic diagram of the apparatus used. It consists principally of nitrogen source and controls, temperature control equipment, measuring devices, gas meters, the mounted cores and the automatic pressure and time measuring devices.

Temperature Control

The control valves, the "surge" cylinder, the core and the pressure transducers were enclosed in a cabinet which was maintained at a constant temperature of 78 ^{o}F by an AMINCO thermostat and electronic relay, whose voltage input was regulated by a powerstat. The upstream and downstream temperatures of the core were measured by two iron flow-line thermocouples, the output voltage of which was measured by a Leeds and Northrup millivolt potentiometer.

Gas Supply, Lines and Controls

Nitrogen gas, which was commercially available at about 2500 pounds pressure was supplied from a tank. Gas lines and fittings were mainly 1/8-inch stainless steel Autoclave, except between the inlet face of the core and the surge cylinder, where 1/4-inch stainless steel tubings and fittings were used. The 1/4-inch tubing was used to reduce pressure loss.

To attain a high degree of pressure control at the inlet side, a small steel cylinder was installed at the inlet flowline. This cylinder was used as a surge outlet for any abrupt pressure changes that might occur in the system. To maintain a constant inlet pressure in a range of 5 to 160 psig a low-range diaphram type Canadian Liquid Air regulator was installed. Where a higher inlet pressure was required,

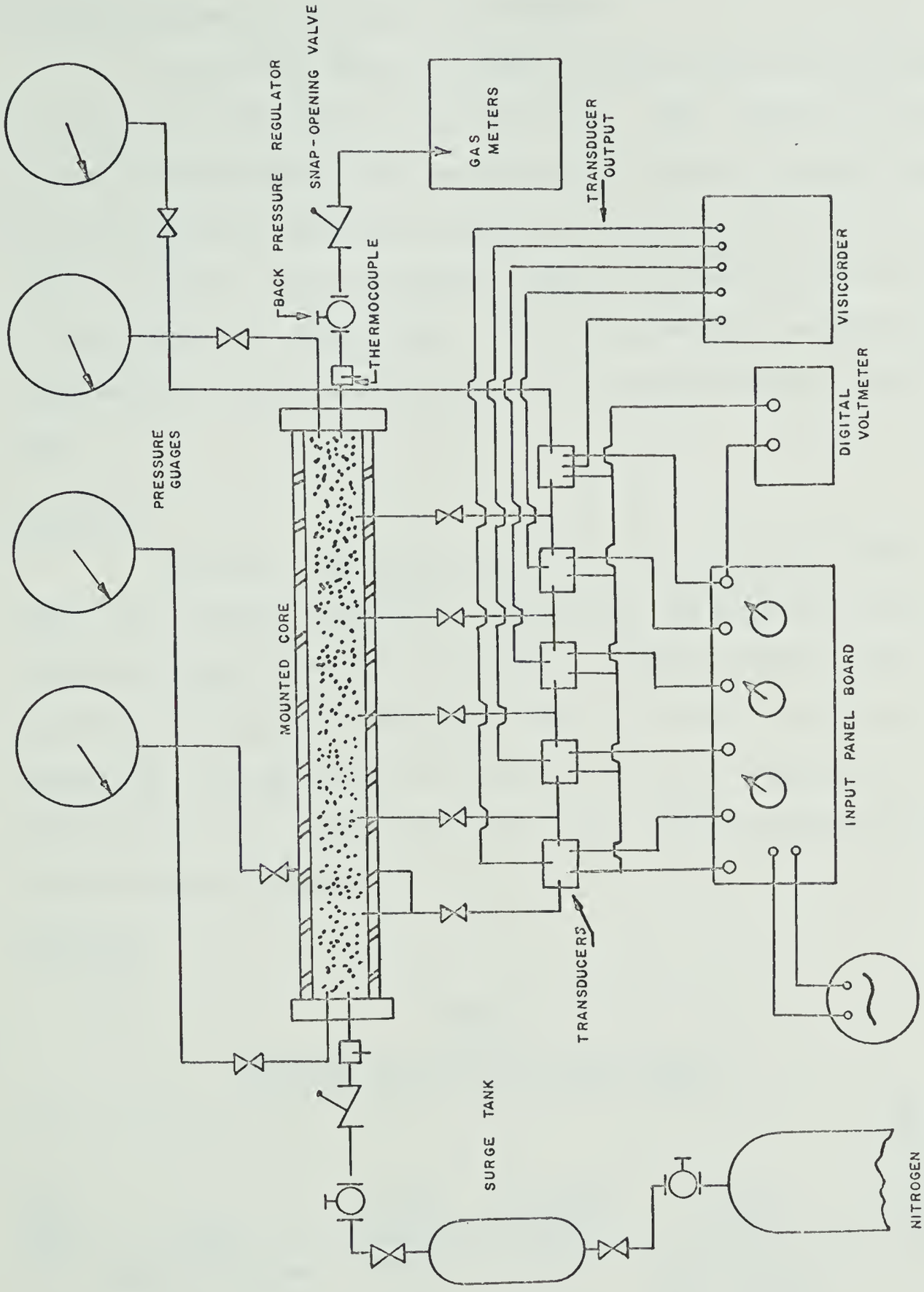

Figure 1. SCHEMATIC DIAGRAM OF PRESSURE TRANSIENT APPARATUS

this regulator was replaced with a high-range supply regulator and a back-pressure regulator shown in the diagram.

At the outlet face a 0 to 2000 psi range back-pressure regulator was used to maintain constant outlet pressure. This, however, was only used in the steady-state flow tests because it required a certain time for the pressure to stabilize, which made it inapplicable to the unsteady-state flow tests. Another important feature of the outlet flow line was the snap-opening or closing valve. This was necessary to satisfy an instantaneous constant outlet pressure at any time beyond the initial time.

Gas Meters

Two types of gas meters were used in the steady-state flow tests. The soap-film displacement burette was used whenever measurements of flow rate ranged from 0.1 to 0.8 SCFH. At higher flow rates the burette was replaced by a calibrated Fisher or Precision Instrument wet test meter. As there was no lower limit on the rate recommended for the Fisher meter, it was calibrated to less than 1 SCFH and checked closely with the burette readings.

The Cores

TABLE 1

Physical Properties of Cores Tested

Core No.	Type	Length (inches)	Diameter (inches)	Core Holder	No. of equally spaced pressure taps
1	Berea Sandstone	36.000	3.500	Epoxy Resin in steel casing	7
2	Alundum	16.535	2.008	Epoxy Resin in Lucite casing	7
3	Limestone Core	5.944	3.500	Epoxy Resin in Steel	2

Table I summarizes the physical characteristics of the cores tested in the experiments. Actually all of the above cores were mounted and prepared by previous investigators but only cores 2 and 3 are mentioned in papers written by Hamilton [25] and Mackett [26], respectively.

Probably because of the length of time that the cores had not been used, a few of the pressure taps and end-plate flow lines were plugged. The end plates were removed, all pressure taps and lines cleaned out and all "O" - rings replaced. The inlet and outlet flow lines of Core 1 were redesigned for higher pressures. In addition, pressure taps were drilled in the faces of the end plates. Cores 1 and 2 were tested at confined pressures of 500 and 200 psig, respectively.

Core 3 was used in the steady-state flow tests to analyze possible mechanical end effects. Two internal pressure taps were drilled as close to the ends as possible. The same core holder designed by Mackett [26] was used for these tests.

Pressure Measuring Devices

The reliability of the pressure transient data was mainly dependent on the pressure measuring apparatus. Non-varying pressures such as the inlet and outlet pressures were measured by calibrated, bourdon-type Heise gauges, while varying pressures which were obtained at precise time intervals were determined with the use of the Stratham PM 80 TC differential pressure transducers. A Kempo SC-18-1 transformer supplied the required line voltage of 16 volts and less. Non-Linear Systems Model 481 digital voltmeter was used to measure input voltage to the transducers. The output differential pressures were recorded on a Honeywell Direct Recording Visicorder Oscillograph. Five pressure transducers were used, four of which were rated for a differential of $\pm$ 15 psi.

The transducer installed nearest the outlet had ± 50 psi allowable differential.

The calibration of the transducers involved the determination of an input voltage and a differential pressure corresponding to a 6-inch maximum deflection on the oscillograph paper. To find that input voltage two alternatives were available. One merely involves a hand calculation of the voltage, using resistances and other data obtainable from the operation manuals of both transducer and recorder. The other involves the application of actual measurable differential pressures across the transducer. Probably because of unaccountable factors in the calculations, the results of the first alternative were found to be quite unsatisfactory. Therefore the second procedure was followed, using a mercury manometer to calibrate each transducer. The details of the calibration process are given in the Experimental Procedure.

EXPERIMENTAL PROCEDURE

Calibration of Transducers

The transducers were very prone to damage to their electrical systems and diaphragms if a specified input voltage and allowable differential pressure were exceeded. In order to insure the safety of the transducers, precautionary procedures of calibration and operation were observed.

Figure 2 shows the calibration equipment. The inlet line and connection to the transducer was made flexible and long enough so it could be connected to all transducers one at a time. The step-by-step procedure of calibration was as follows:

1. The approximate maximum allowable input voltages to the transducers were precalculated using pertinent data from the manufacturers' catalogues. These gave an approximate safe range of voltages that could be applied to the transducers.
2. With the power supply on, a voltage lower than the calculated maximum allowable (about 1/3) was applied across the transducer, controlled with rheostats on the panel board.
3. With the high and low sides of the transducers open to the atmosphere, the transducer output light indicator was set to the zero line of the oscillograph paper, by adjusting the corresponding galvanometer in the Visicorder.
4. With the low side of the transducer always opened to the atmosphere, pressure was gradually applied on the high side until the manometer read 30 inches of mercury. If the applied input voltage to the transducer was too high the light indicator went out of bounds. The 6-inch deflection was obtained by further increasing or decreasing

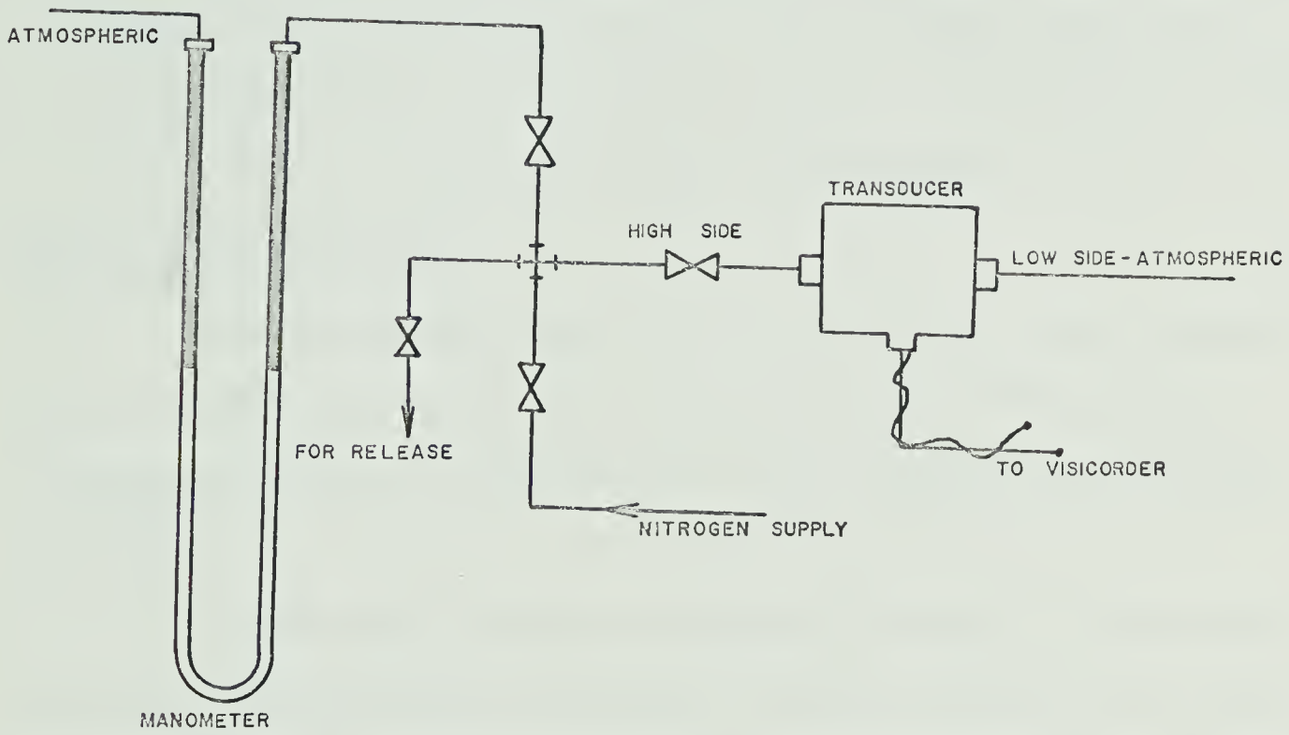

Figure 2. SCHEMATIC DIAGRAM OF CONNECTIONS FOR TRANSDUCER CALIBRATION

the input voltage. In the case of the 50 psid transducer a deflection corresponding to a manometer reading of 60 inches of mercury was obtained.

5. Finally, to obtain the calibration factor, at least 5 pressures from 0 to about 15 psig were applied and the corresponding deflections measured. These pressures were then plotted against the deflections, resulting in a straight line. The slope of this line was the calibration factor for that input voltage. The oscillograph division of 0.1 inch was taken as the unit of deflection.

Operation of Transducers

The transducers could be used up to absolute line pressures as high as 5,000 psi provided the total pressure drop across all the transducers would not exceed the sum of their allowable differential pressures.

A fail-safe procedure followed was to open all valves interconnecting the transducers during the time that pressure in the core was building up. This reduced the pressure differential across any transducer to zero during build-up to high pressures. When the desired pressure in the core was reached, the interconnecting valves were then closed.

Determination of Effective Porosities

Three cylindrical samples were cut from scattered points of a 3-foot Berea Sandstone, and another two from a piece of an Alundum Core. Calibrating blanks were also cut from a 3/4-inch diameter steel rod. All pertinent dimensions of the cores and the blanks were averaged from caliper measurements. Using these data and procedures which are standard

for the Boyle's Porosimeter, the porosities were determined and recorded in Table 1A of the Appendix II.

Steady-State Flow Tests and Permeability Determinations

A series of steady-state flow conditions were imposed on a sample at varying pressures. In each test, flow rate and pressures at inlet, outlet, and at all pressure taps were measured. The steady-state condition of flow was easily observed from the Visicorder output. When flow became steady all output indicators of the transducers gave straight line traces. The distances of these lines from the zero line were measures of the pressure drops across the sections of the cores to which the transducers were connected.

In the measurement of gas flow, the soap-film burette was employed in measuring low flow rates. It was used as long as it was possible to obtain accurate travel time of the bubble in the burette. At higher ranges, the burette was replaced with the wet test meter.

To determine the permeability distribution along the core, pressure-squared was related to position. Sections of the core which were shown to have straight line relationship were considered homogeneous. Permeabilities were determined using the Klinkenberg extrapolation method, as modified by Dranchuk and Sadiq [27]. A flow regime graph was prepared by plotting pressure-squared drop versus flow rate. The data points in the viscous flow region lie on a 45^{o}-line segment starting from the low flow rates to a point which marks the lower limit of the visco-inertial flow region.

In addition, the flow regime plot above was also useful in delineating the experimental range where the unsteady-state tests were run. Knowing the point where visco-inertial flow starts, only pressure

drops resulting in flow rates lower than this critical value were imposed on the core to be sure that no turbulent flow occurred.

Unsteady State Flow Tests

Pressure Drawdown Case

To initiate a drawdown test, the desired initial pressure was controlled at the upstream side of the core, while the outlet valve was closed. The equalized pressure inside the core was observed from the inlet and outlet gauges and also from the Visicorder. When pressure had stabilized, all the transducer output light indicators appeared as a point tracing the zero line on the Visicorder.

The case of a finite boundary with influx was achieved by performing a test with the upstream valve opened. On the other hand the finite boundary without influx was accomplished by having the same valve closed. The third type of boundary condition, the infinite boundary, was studied during the period before the pressure transient reached the inlet boundary. The isolation and analysis of this third case was possible because the transient time to reach the inlet section was obtained both from the oscillograph paper and the inlet pressure gauge. In the case of the finite boundary without crossflow, additional data obtained were the inlet pressure readings at predetermined time intervals.

In measuring flow rates, time intervals were first selected at which the cumulative readings on the wet test meter were marked and read. It was found out that a time interval of 5 seconds was sufficient for an observer to obtain fairly accurate readings.

Pressure Buildup Case

The initial preparations for the test, the manipulations of the transducers and recorder, and the simulating procedures for the three types of boundary conditions were exactly the same as those described in the pressure drawdown tests. The buildup test, however, differs in that 1) initially, a steady state flow was induced in the core; 2) in accomplishing the test, the outlet valve was abruptly closed; and 3) as there was no flow to measure, the corresponding data obtained were the pressure readings at the outlet face, read at pre-selected time intervals.

To summarize, the initial preparations and observations made prior to taking any test included the following:

1. preparation of thermocouples and potentiometer.
2. control of cabinet temperature to 78°F.
3. control of gas flow according to the desired rate and pressures.
4. adjusting input voltages of transducers to the calibrated valves.
5. adjustment of transducer output indicators to the zero line.
6. admission of gas inside the transducers, closely observing the precautions discussed previously.
7. selection of a convenient reference pressure for the 50 psid transducer.

The consolidated data for an unsteady-state test included the (1) cabinet temperature, (2) barometric pressure, (3) initial and final values of the input voltages to the transducers, (6) cumulative flow rate (for drawdown tests), (7) reference pressure, (8) time of transient

from outlet to inlet face as observed from Heise gauge, (9) number of deflection divisions for each pressure tap at particular recorded times.

A computer program was written to evaluate experimental pressure in psia and also the square of the pressure for each pressure tap at any time interval considered. The data included were time and the corresponding deflection (divisions) for each of the pressure taps, the reference pressure and the atmospheric pressure. The program has been included in the Appendix.

DISCUSSION OF RESULTS

The experimental equipment was found to be satisfactorily designed for the analyses of transient flow through porous media. Although the overheating of the visicorder resulted in some appreciable changes in the voltage input to the transducers, no change was noted on the pressure recording oscillograph paper. On the other hand, even a very slight change in pressure differential across the transducer was instantaneously recorded with no noticeable effect on the imposed voltage. The procedure of calibration adopted for the transducers solved this problem of being pressure - but not voltage-sensitive, which was the main complaint of Mackett [26] in his use of one transducer.

In his attempt to use cores with diameters greater than one inch, Hamilton [25] concluded that there were voids created between the core and resin material and also between the resin and casing during the process of mounting. He also contended that cores of this size were susceptible to cracks and permanent deformations in the resin after application of a relatively high pressure. However, for the two cores used in this work, the mere fact that transients were observed and recorded in every section between any two pressure taps confirmed that these defects were not present. Their presence in the core would surely have provided direct communication between pressure taps.

On the other hand Mackett [26] observed that the epoxy resin, when poured into the annulus, had a certain degree of penetration into the core. From specimens closely examined, this penetration had the advantage of improving the interface between the core and the resin. However, it has the particular disadvantage of reducing the effective diameter of the core, the measurement of which would also pose another problem.

It was initially decided to perform unsteady-state tests at an inlet pressure beyond 165 psig and the outlet above atmospheric pressure, but problems of pressure control were encountered. Appreciable pressure fluctuation was observed at the inlet in the case of the draw-down tests, and at the outlet, in the case of the buildup tests. The inability to control pressure in these ranges may be attributed to the very wide ranges of both the supply valve regulator and the back pressure regulator. Tests were therefore performed below 165 psig.

Experimental Results

(1) Steady-State Flow Tests

Initially all test results were evaluated by relating pressure-squared against the length of the cores, which were tabulated in Table $2A_1$ and $2A_2$ of the Appendix and plotted in Figures 3 and 4 respectively for Core 1 and Core 2. The relationship for the Berea Sandstone shows excessive pressure drops occurring both at the inlet and outlet sections as compared to the Alundum core. A ready explanation for these pressure drops was a mechanical end effect, resulting from the machining of the core faces. To investigate further this end effect, similar steady-state flow tests were run using Core 3, which was one of the limestone cores prepared by Mackett [26]. The faces of this core were also machined. Pressures were measured at four points, two at the faces of the core and two from internal pressure taps. The data and results are tabulated in Table 3A of the appendix. The results show the same unproportionate pressure relationship as shown in Figure 2A of Appendix I. Apparent permeabilities were calculated using both the pressures read at the faces and the pressures measured internally. Of the 20 runs, the average

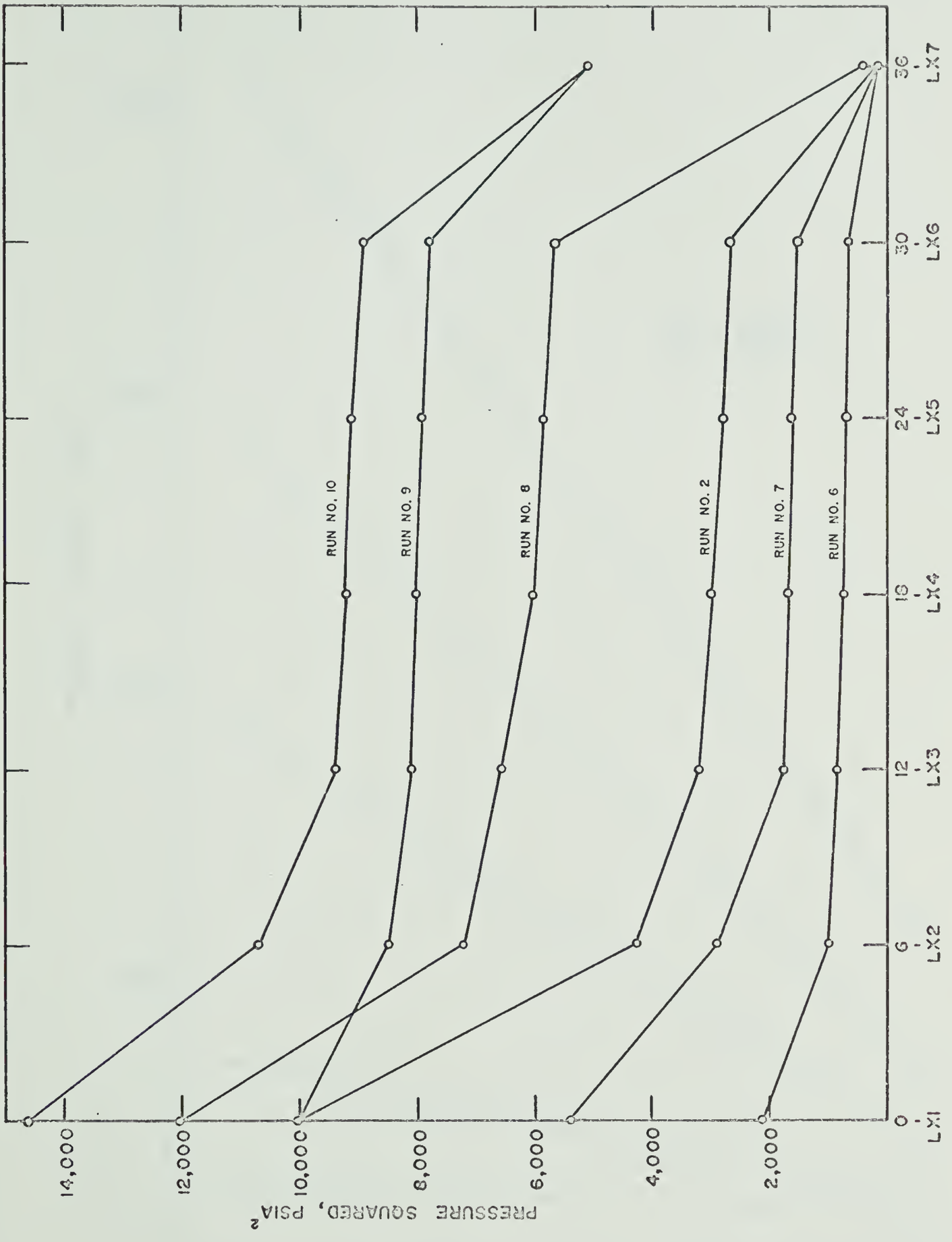

Figure 3. STEADY FLOW RUNS FOR BEREA SANDSTONE, CORE 1; PRESSURE SQUARED VS. CORE LENGH AT 78°F.

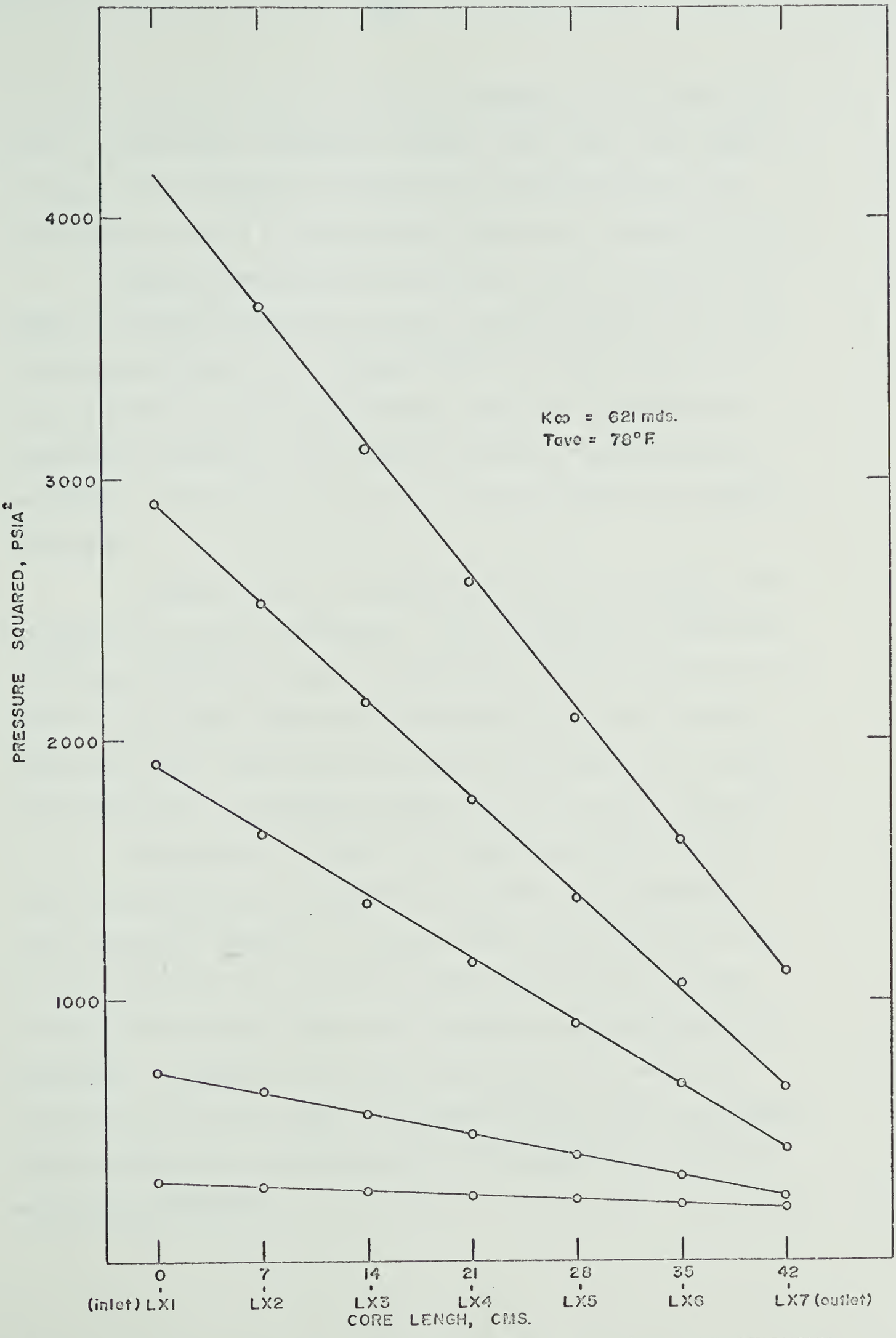

Figure 4. STEADY STATE, PRESSURE SQUARED VS. CORE LENGTH RELATIONSHIP FOR THE ALUNDUM CORE.

difference of the two sets of calculated permeabilities was about 67%, with a few individual differences as high as 95%, found at low mean pressures. The Klinkenberg permeabilities determined from the two sets of data on Core 3 are illustrated in Figure 3A, and differ by 31%.

Another valid possibility which may be used to explain this damage on the Berea Sandstone core was a possible exposure of the core to moisture or fresh water. Studies [33,34] have shown that the presence of fresh water in Berea Sandstones results in a considerable reduction in permeability. No complete history of the Berea core is available to show, that at no time, has it been exposed or in contact with water.

If damage was due to mechanical end effects, its depth would be limited to a few grain diameters. Upon this basis, one observation from Figure 3 appears to favor the fresh-water theory in explaining this damage. Of the five internal pressure points in the core, the point nearest the outlet (LX_2) was not co-linear with the other four points. This suggests that the damage was deeper than a "few grain diameters."

Referring back to Figure 4 the resulting pressure versus length relationship for the Alundum Core verified the straight-line graphs obtained by Hamilton [25] in his tests of the same core. Like the Berea Sandstone core, the faces of this core were also machined. A perusal of the results indicates no pressure drop attributable to any damage. If damage in the Berea core was due to the mechanical preparation of the core, these test results on the Alundum core suggest that end effects due to machining become less significant as the core becomes more permeable.

The damaged ends of the Berea core (Figure 3) seem to render meaningless any pressure transient initiated outside the inlet or outlet faces of the core. However, from the concept of permeability, the average permeabilities in the damaged sections may be understood as some form of pseudo-permeabilities at the inlet and outlet sections. These equivalent permeabilities were evaluated by assuming a linear distribution of pressure-squared at the end sections as shown in Figure 3, although this assumption may be far from the actual pressure distribution. Therefore, for Core 1, three sections were assumed as having different permeabilities: namely, the inlet section (Lx1 to Lx2), internal section (Lx2 to Lx6) and the outlet section (Lx6 to Lx7).

In the determination of permeabilities by the Klinkenberg extrapolation method, the same basic equations applied by previous investigators [25,26,28] were used. Figure 4A shows the difference of pressure squared versus flow rate relationship for Core 1. Figure 5A shows the apparent permeability versus 1/Pm relationship. To establish the best Klinkenberg plot in Figure 5A only those points falling on a 45^{o}-line as illustrated in Figure 4A were considered. From Figure 5A, the extrapolated permeabilities for the inlet, internal and outlet sections of Core 1 were respectively 1.24, 18.90 and 2.24 millidarcies, and from Figure 6A, the calculated permeability for Core 2 was 621 millidarcies. Apparent gas permeability data and results are tabulated respectively in Tables 4A and 5A for Cores 1 and 2.

The relationships for the Berea sandstone shown in Figure 4A indicate that an assumption of viscous flow condition was justified. Free molecular flow generally occurs at very low pressures. A criterion

for this flow according to Wilson [29] is that the ratio "average pore radius/molecular mean free path" must be less than unity. This ratio was evaluated to be 6.5 for a compact-crystalline limestone with a permeability of 0.1 millidarcy, porosity of 7% and using nitrogen at 32°F and 1 atmosphere. Under test conditions, this ratio would become higher since the average pore radius of sandstone in Core 1 is greater than that of limestone, and the operating pressures used were above one atmosphere. Thus, the molecular mean free path would be less. Turbulent flow has been ovserved [25,26,28] in cores with porosities and permeabilities of the same magnitude as those of Core 1 at pressures higher than those encountered in this work. A perusal of Figure 4A verifies that turbulent flow condition did not exist in these tests.

For the Alundum core, the data observed were compared together with those of Hamilton [25] for the same core. Figure 5, relating pressure-squared difference versus rate, clearly shows the point of deviation for the 45°-line which marked the start of the visco-inertial regime. This point corresponds to a flow rate of 23.0 SCFH and a mean pressure of 57 psig determined from the Klinkenberg plot in Figure 6A.

(2) Unsteady-State Flow Tests

The analysis of pressure transients, whether obtained theoretically or experimentally, depends on the ability to define or evaluate many of the variables affecting flow. In general the pressure relationships in a core with gas as a medium are functions of temperature, viscosity and compressibility of the gas, porosity and permeability of the core, distance and time. From previous discussions of the properties used in the experiments, porosities and viscosity were essentially constant within the experimental test range. Therefore, the

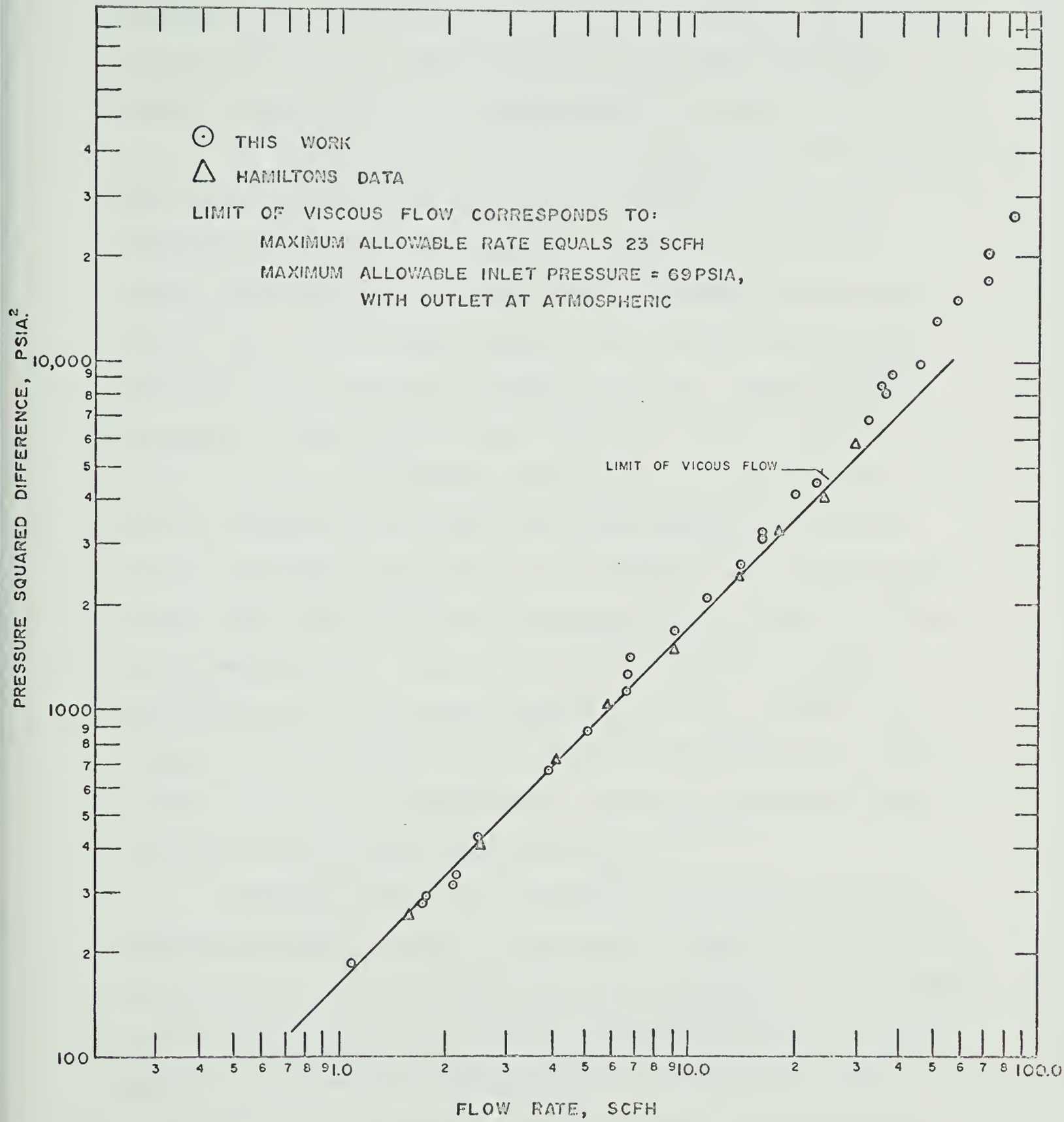

Figure 5. FLOW REGIME PLOT, ALUNDUM CORE

permeability variations along the core, determined from steady flow tests, could then be correlated with pressure transients. The influence of these variations was evaluated by relating pressure with time or distance along the core for a particular type of boundary condition.

To analyze pressure transients in Cores 1 and 2 qualitatively, both for the infinite and finite boundary conditions, the pressure distribution versus time was correlated. Tables 6A and 7A are the results of the experimental drawdown and buildup tests, respectively. Figures 6 and 7 show pressure drawdown curves obtained from the Berea Sandstone for the two types of boundary conditions. Similar drawdown curves were obtained for the Alundum Core and are shown in Figures 8 and 9. The two sets of drawdown curves which were super-imposed in Figure 9 correspond to the same initial conditions, but of different boundary conditions. For buildup tests, Figures 10 and 11 show pressure buildup curves taken from Core 1 for the same type of boundary conditions as the drawdown tests. Figure 12 is a buildup test on the Alundum Core for the case of an external boundary of constant pressure. No buildup test corresponding to the no-influx case was conducted on the Alundum core because of the difficulty of obtaining simultaneous gauge readings at the inlet and outlet of the core.

Referring to Figure 6, the drawdown curves drawn for the no-influx case provide a picture of how pressure declined at each position of the core. It was at the early stage of the transient that the largest pressure drops occurred. The nature of the pressure decline is better observed in the drawdown curves of Figure 7A which show that each position of the core (except the outlet) followed an almost parabolic decline. The boundary case of no-influx at inlet implies, according to

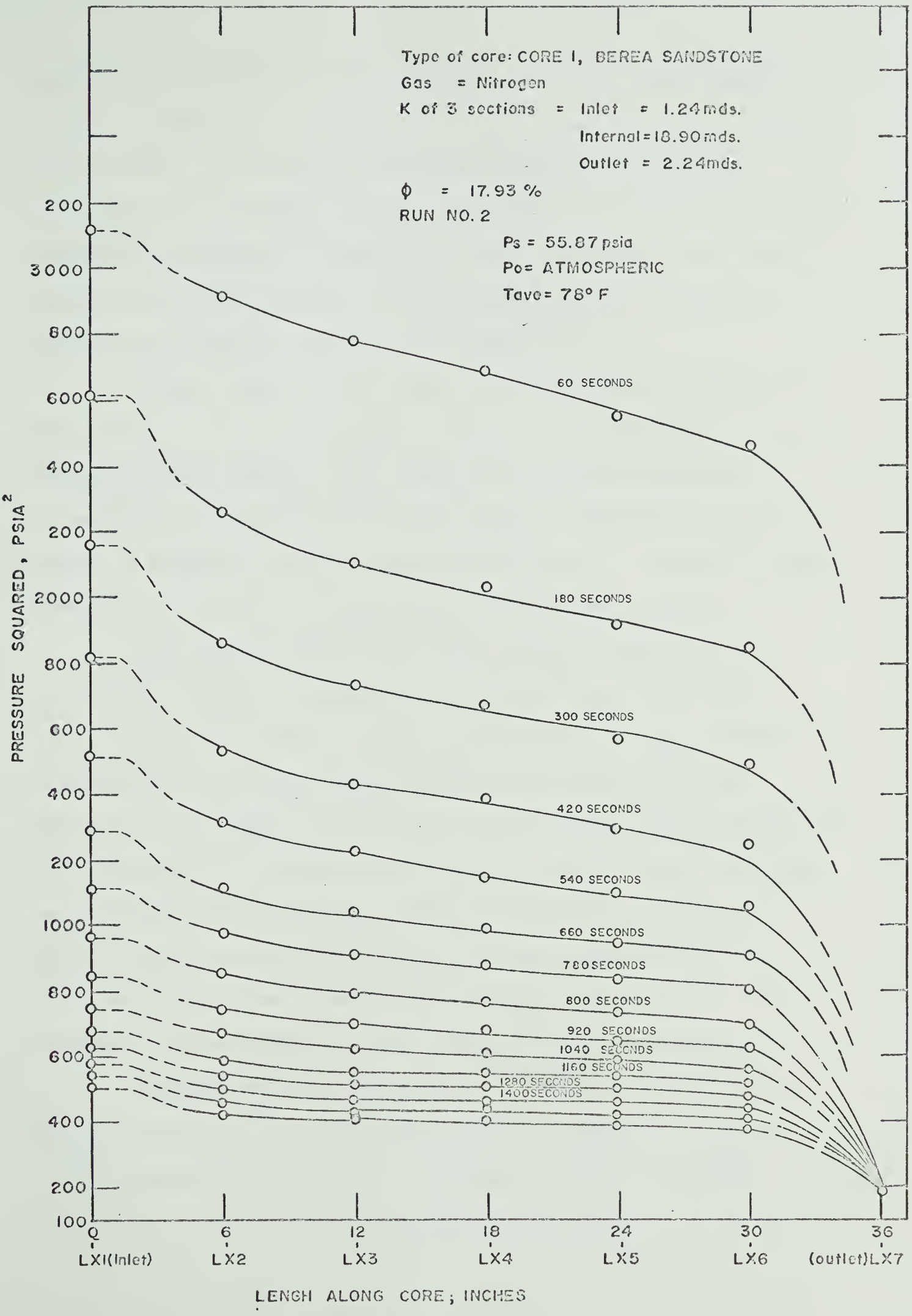

Figure 6. PRESSURE DRAWDOWN, P^2 vs X, NO-INFLUX CASE

Darcy's Equation, that the pressure gradient at the external boundary was zero. Graphically, the portions of the p^2 versus x curve at the inlet section should be horizontal. No pressure measurements were made within the Inlet and Outlet sections. As such, it was impossible to determine the pressure distributions at these end sections, and consequently, the pressure gradient at the boundaries. These portions of the curves were dashed as shown in the figure.

Figure 7 shows drawdown curves for the infinite boundary case, that portion of the constant external pressure case before the transient reached the inlet boundary. For comparison, drawdown curves also corresponding to the period before the transient reached the inlet were plotted in Figure 8A for the no-influx boundary case. Although the applied pressures were not the same, qualitatively the curves are similar.

The irregularities in the above transient curves for Core 1 were evidently due to the variation of permeability over the length of the core. In order to obtain a qualitative comparison of the influence of permeability variation, similar drawdown curves were plotted in Figure 8 for the Alundum core which was already shown to be of uniform and high permeability. In general the transients obtained from the Alundum core were free from sharp pressure changes observed in the sandstone system. The series of pressure drawdowns clearly shows the progress in approaching the steady-state condition which is shown as essentially a straight line connecting the inlet and outlet sections of the core.

The superimposed drawdown curves in Figure 9, also of Core 2, show a comparison of the two boundary cases of no-influx and constant external pressure for the same initial inlet pressures. It may be observed from these results that during the early period of the transients,

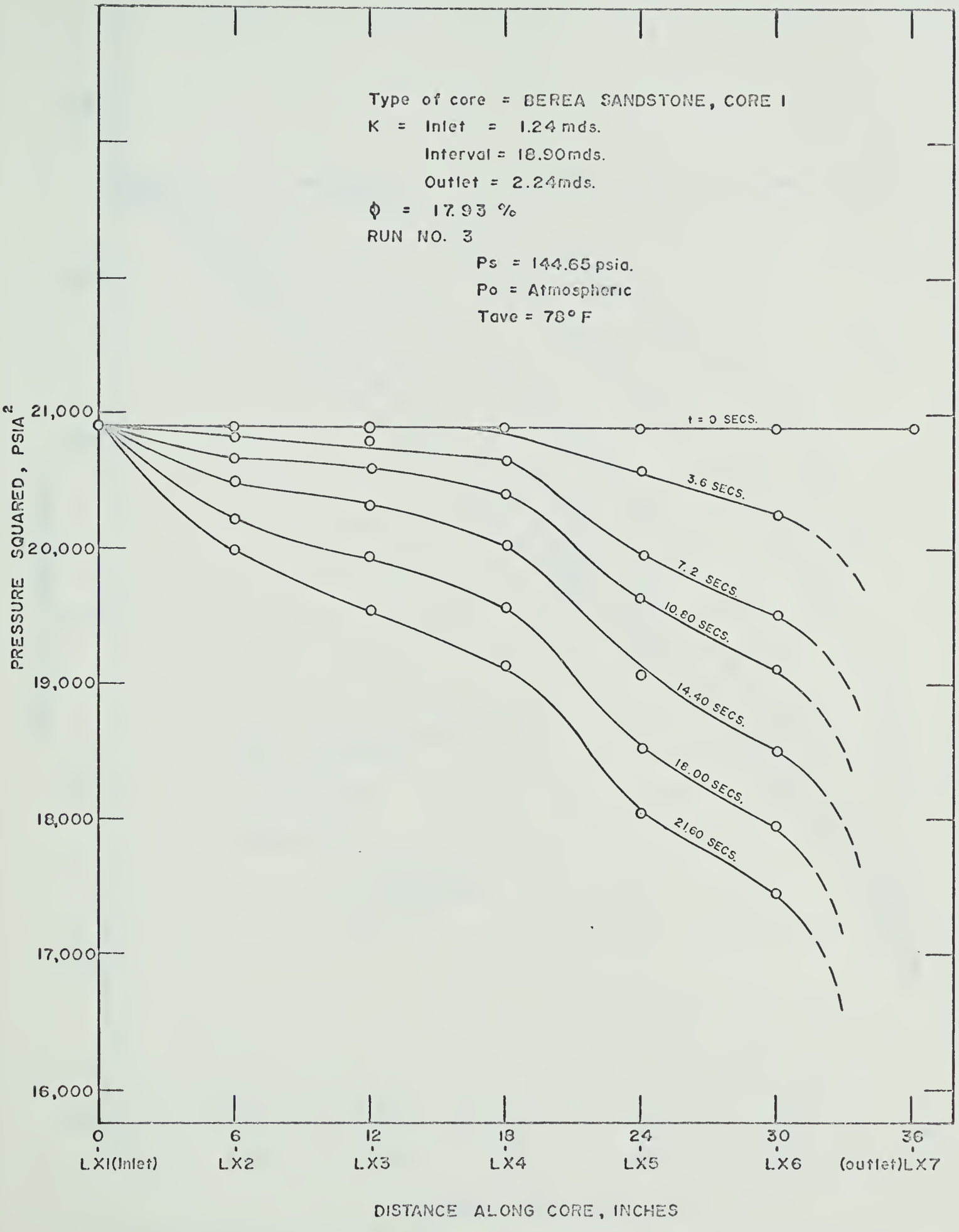

Figure 7. PRESSURE DRAWDOWN, P^2 vs X, TAKEN BEFORE RESPONSE WAS RECORDED AT LX2 FROM CONSTANT INLET PRESSURE CASE.

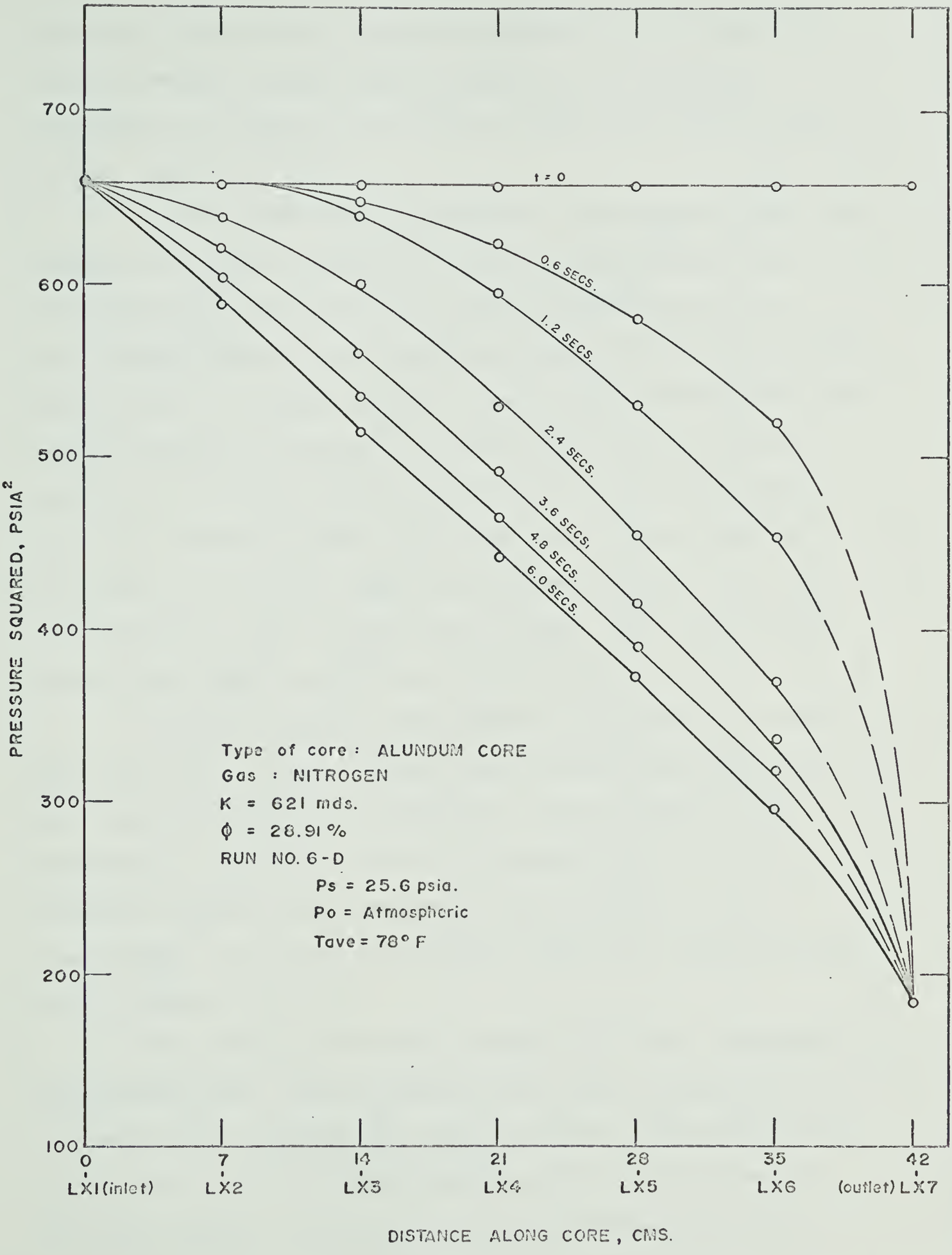

Figure 6. PRESSURE DRAWDOWN, P^2 vs X, CONSTANT BOUNDARY PRESSURE CASE

deviations between the two cases were negligible near the outlet but increased towards the inlet and with the time of the transients. Furthermore the drawdown curves for the no-influx case exhibit a zero pressure gradient at inlet.

In both cores tested for drawdown, it has been noted that the time for the pressure transient to be observed at an upstream point along the core was affected by the pressure drop imposed across the core. Figure 9A shows this relationship as determined from the drawdown tests of Core 1. The right ordinate is the recorded time when the first pressure change was observed at the inlet face, while the left hand ordinate corresponds to the time the transient reached the pressure tap (Lx2) 6 inches from inlet. For a particular pressure drop, the difference of the left and right hand ordinates represents the travel transient time of the 6-inch long inlet section. This section of the core has a much lower permeability than the internal section.

From the cumulative gas production, instantaneous flow rates were calculated and plotted against cumulative time (see Figure 10A). The results are typical of an exponential flow rate decline. This phenomenon is significant in that if turbulence were to occur at a particular unsteady-state flow rate it would be during the early stage of flow. The sharp rate of decline suggests the temporary nature of this turbulent condition.

The buildup curves shown in Figure 10 for Core 1 correspond to the no-influx case. Initially gas was made to flow through the system at a steady-state condition after which the gas was simultaneously and abruptly shut in at both inlet and outlet. The series of curves in the figure describe a situation where the section near the outlet

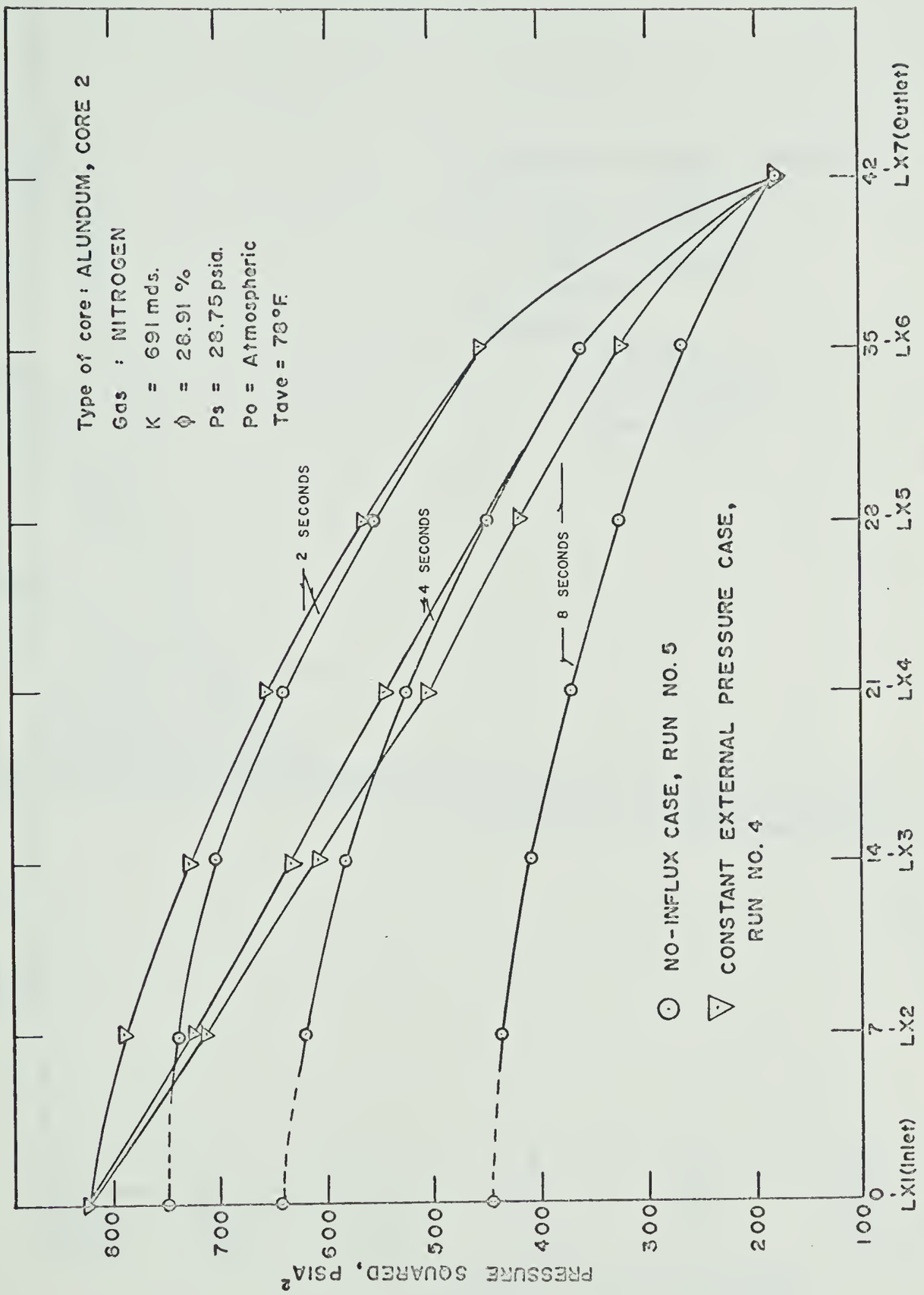

Figure 9. COMPARISON OF THE NO-INFLUX AND CONSTANT INLET PRESSURE CASE, DRAWDOWN

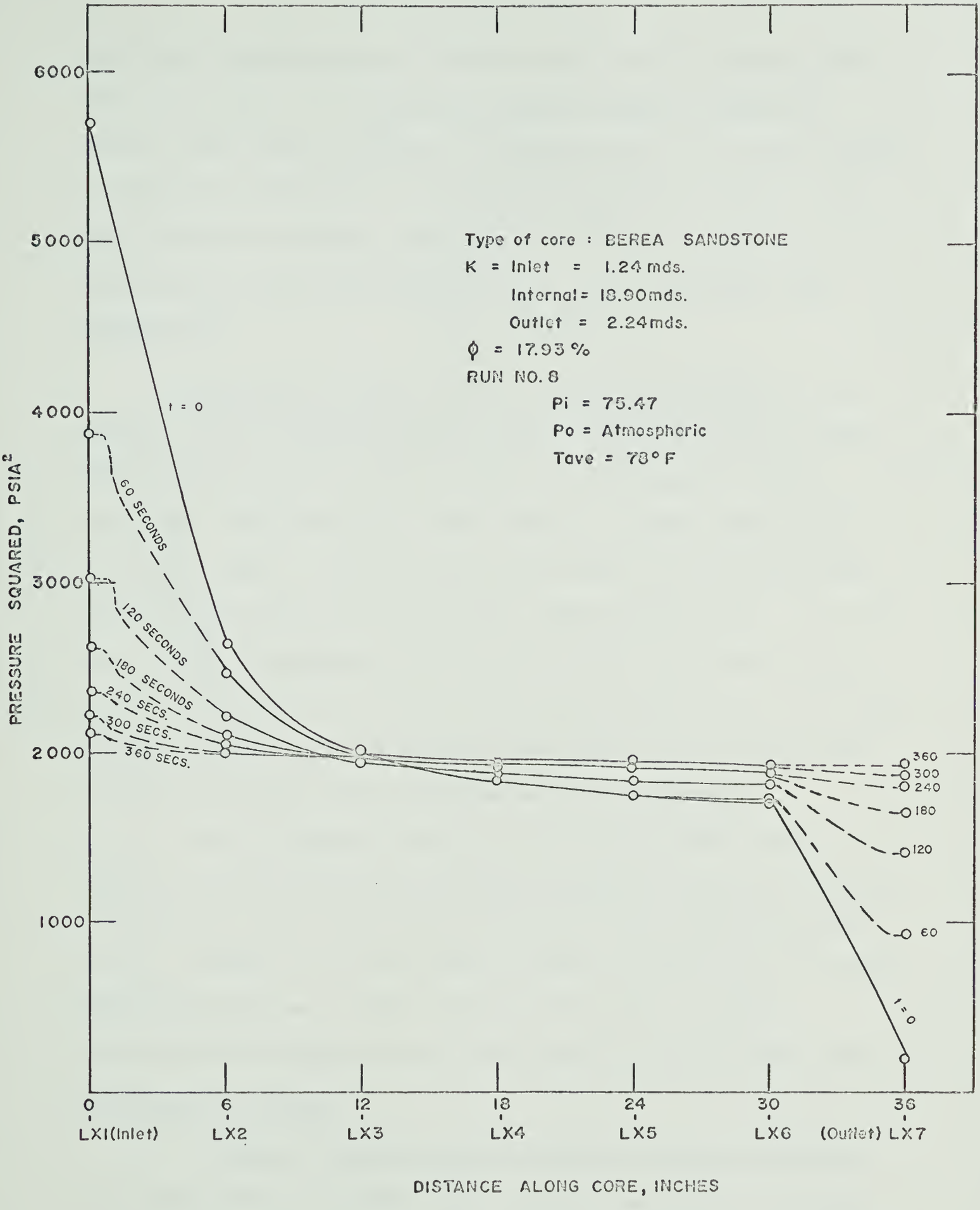

Figure 10. PRESSURE BUILDUP, P^2 vs X , NO-INFLUX CASE

experienced a buildup while the section near the inlet exhibited drawdown to the value of the stabilized pressure, which was below the initial inlet boundary pressure. As a consequence, the internal section of the core was subjected to less changes of pressure compared to the inlet and outlet sections. These phenomena are better described for each position of the core in the pressure - time relationship shown in Figure 11A.

The pressure buildup curves in Figure 11 correspond to the boundary case of constant external pressure and were run with the same inlet boundary pressure as the no-influx case in Figure 10. Some significant observations were noted, namely: 1) a much longer period of time was needed to achieve stabilization than in the no-influx case. The stabilized pressure was the initial inlet pressure itself. 2) The large pressure increments at each position of the core (except inlet) occurred during the early stage of the transient and the rate of pressure buildup diminished as it approached stabilization. These observations correlate with those made on the drawdown curves of Figure 6.

From the pressure buildup curves for the Alundum core in Figure 12 and 12A, basically, observation similar to those in the Berea sandstone can be made regarding the rate of pressure buildup throughout the core. However, its more uniform and higher permeability and porosity would explain the more regular pattern of the curves. Complete stabilization throughout the core was attained in a much shorter time.

(3) Numerical Analysis

A computer program was set up only for the pressure drawdown tests of the infinite boundary case, obtained from the Berea sandstone. In the computation, the core was assumed to have three sections, namely

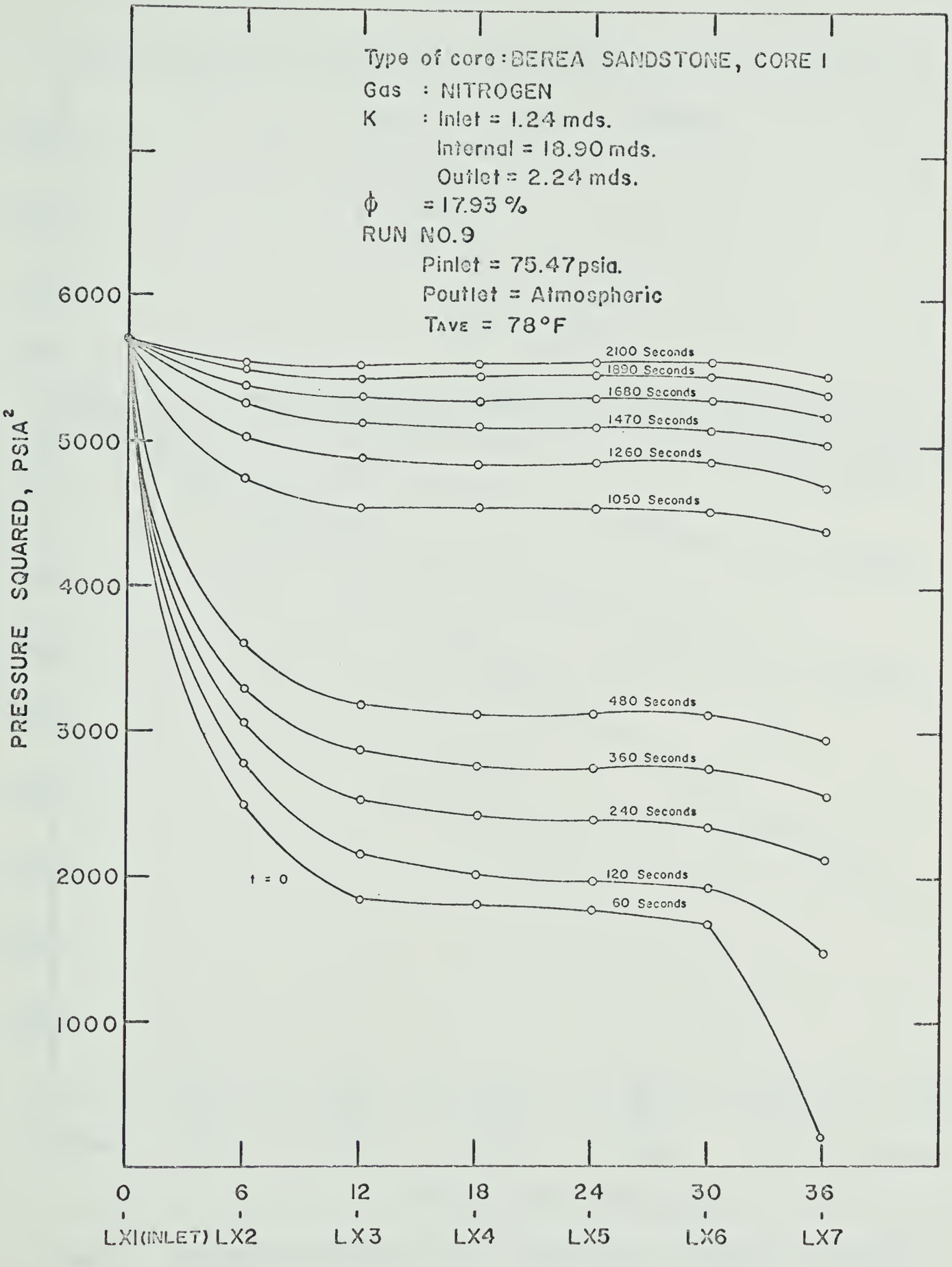

Figure II. Pressure Buildup, P^2 vs X, Constant Pressure Boundary Case

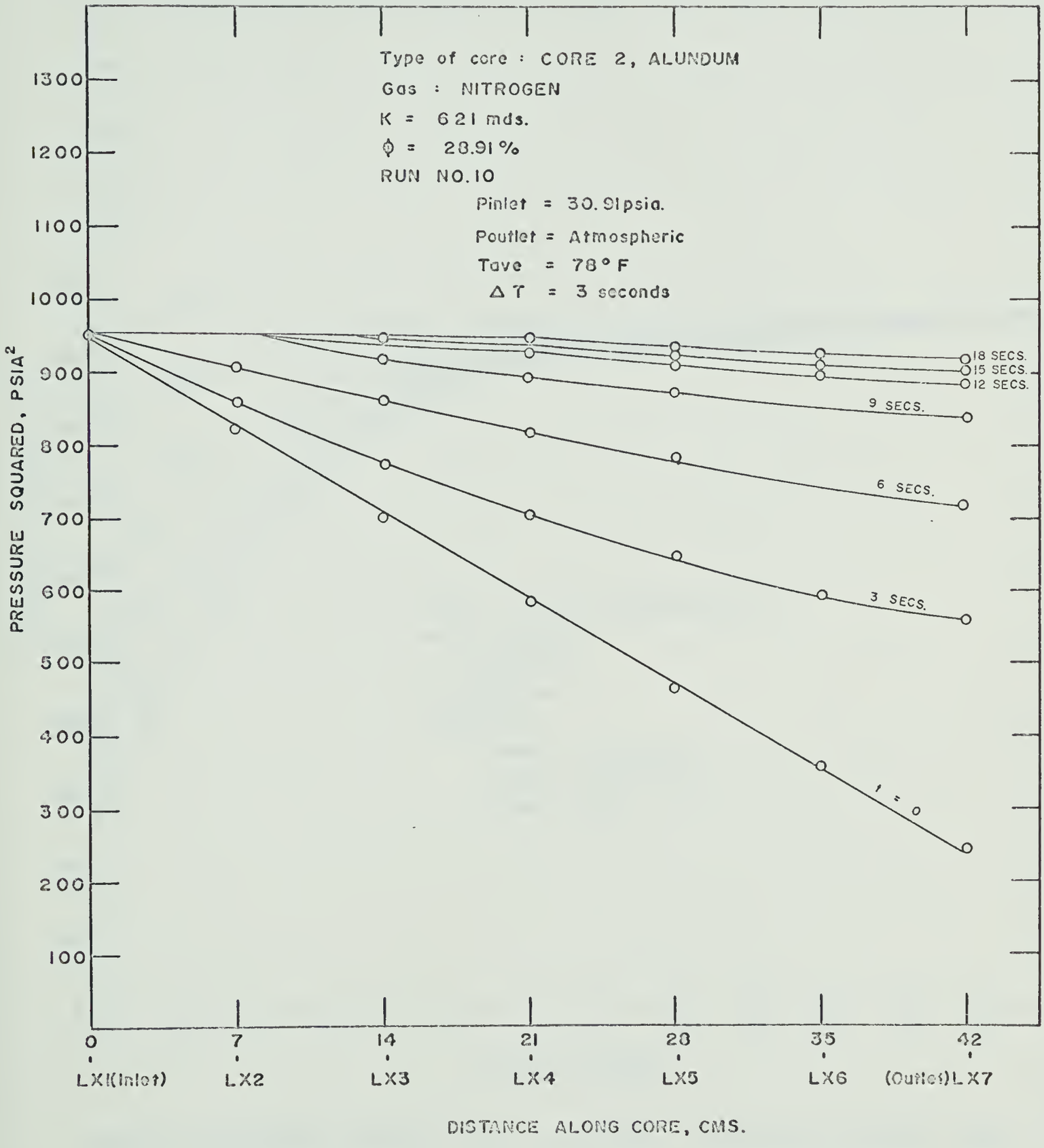

Figure 12. PRESSURE BUILDUP, P^2 vs. X, CONSTANT BOUNDARY PRESSURE CASE

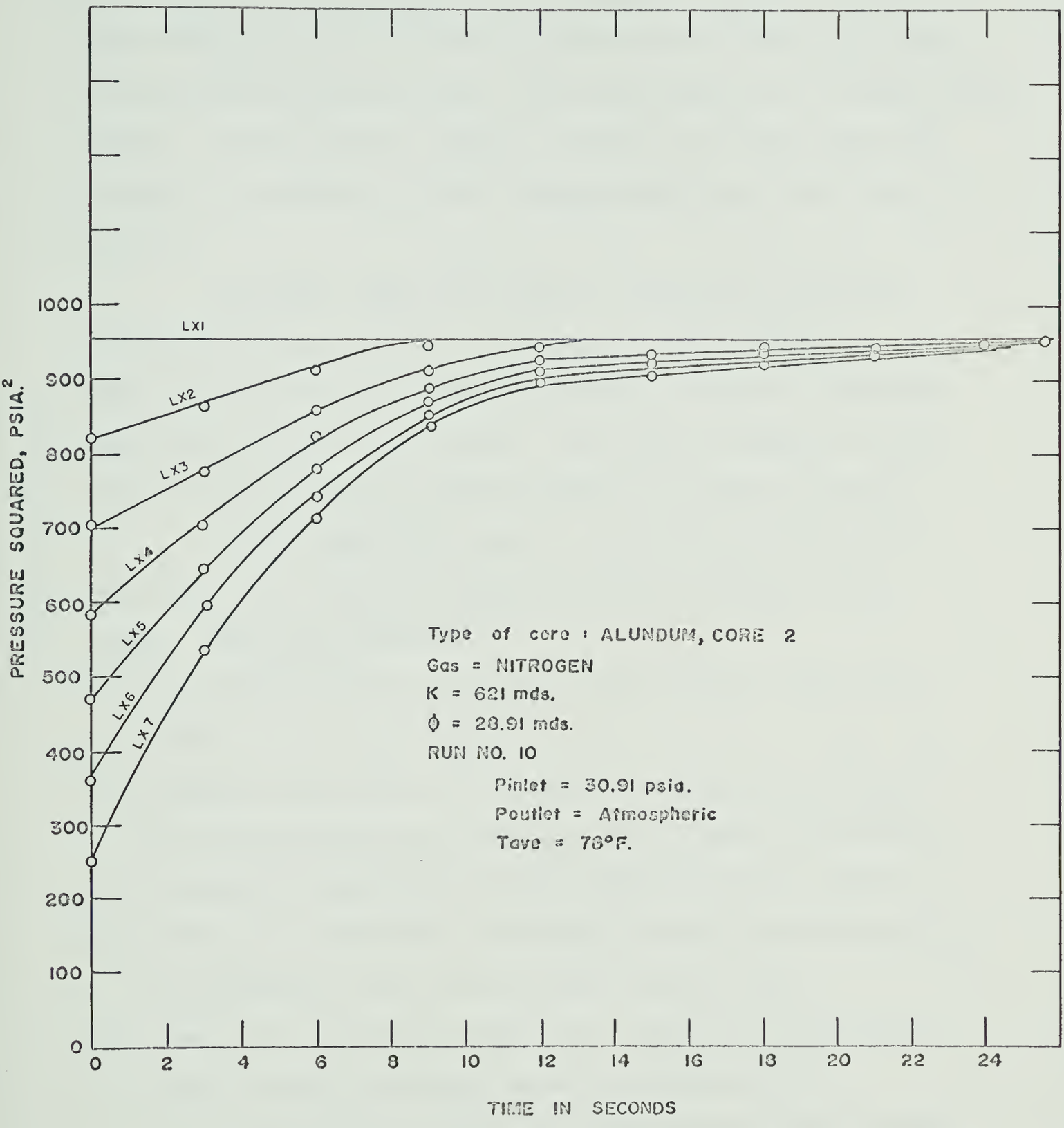

Figure 12A. PRESSURE BUILDUP, P^2 vs. T, CONSTANT BOUNDARY PRESSURE CASE.

the 6-inch inlet section, the 24-inch internal section and the 6-inch outlet section, all of different but sectionally constant permeabilities. Given the initial and the boundary pressures for each run, the pressure distributions along the core were solved and compared with the experimental results. The data and the numerical solutions are given in Table 8A. In Figure 13, numerical solutions and experimental values are shown for Run No. 1.

In general, there were differences between the calculated and the experimental results, ranging between zero and 5% in the test where low pressures were imposed, and zero and 15% in the tests where high initial pressures were imposed. The maximum differences between numerical and experimental results for the run in Figure 13 was 11%.

Further comparisons, however, between the calculated and experimental results showed discrepancies which followed a general pattern. They were as follows:

(1) The numerical solutions were always lower than the experimental values.

(2) Negligible differences or discrepancies between the calculated and the experimental were exhibited near the inlet but gradually increased to appreciable magnitude towards the outlet section.

(3) Further, the differences or discrepancy between the calculated and the experimental curve increased with transient time.

(4) Finally, the differences between the calculated and experimental curve increased with higher initially imposed pressures.

A way to explain each of the above patterns of discrepancies between the two results would be to consider the assumptions and equations upon which the experimental tests and numerical computations were based.

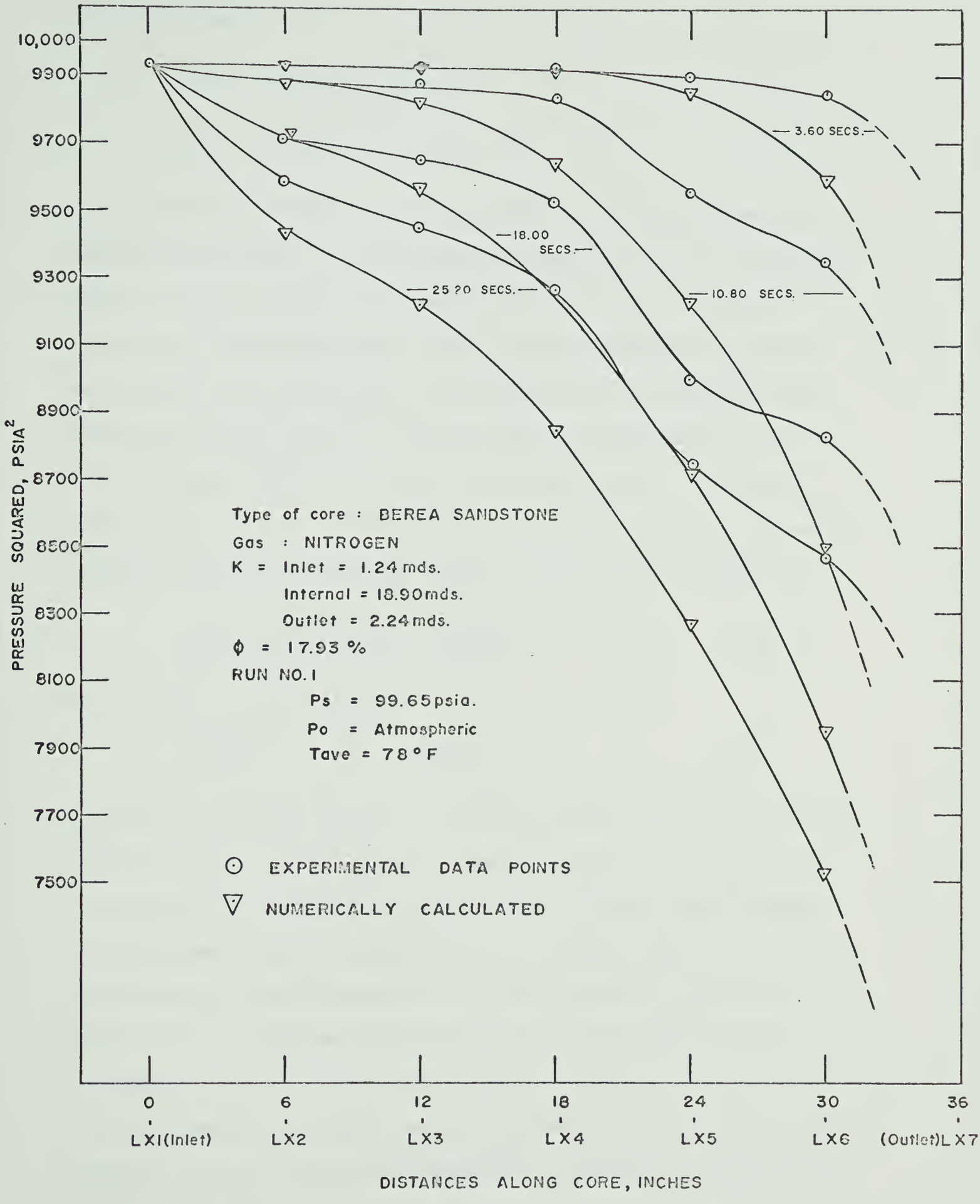

Figure 13. COMPARISON OF EXPERIMENTAL RESULTS AND NUMERICAL SOLUTIONS FOR DRAWDOWN TESTS, INFINITE BOUNDARY CASE

By Darcy's Law:

$$q_N = - \left((K/\mu) \partial P/\partial x \right)_N \qquad (14)$$

$$q_E = - \left((K/\mu) \partial P/\partial x \right)_E \qquad (15)$$

where subscripts E and N refer respectively to the experimental and numerical quantities. The Klinkenberg permeability (i.e. an absolute value) was selected for use in Equation (14), whereas the permeability applicable to the experimental results was an apparent value which varied with the mean pressures. From Equation (4) the apparent permeability is always greater than the absolute permeability. This was shown by Kolada [32] when he proved that the factor (1 + b/Pm) was greater than 1.2 even at the highest mean pressure condition he tested. Equating rates and simplifying, Equations (14) and (15) reduce to

$$(\partial P/\partial x)_N = K_{app}/K_{abs} \quad (\partial P/\partial x)_E \qquad (16)$$

which gives the relationship

$$(\partial P/\partial x)_N > (\partial P/\partial x)_E \qquad (17)$$

Equation (17) suggests that for a drawdown process, the pressure drop measured from the initial pressure would be greater in the numerical calculation, and it therefore explains the calculated values being generally lower than the experimental. The second observation of the discrepancy increasing towards the outlet is merely a consequence of Equation (17). From the relationship, the pressure drop dP (and consequently the difference between the two pressure drops) is proportional to the distance dx measured from the inlet where the initial and boundary pressures for the numerical and calculated quantities are the same and their difference zero.

For the third observation, considering a particular point of the core between any time t_1 and a later time t_2, the mean pressure Pm at t_1 would be higher than that at t_2. By Equation (4) the apparent permeability is lower at t_1. The absolute permeability being constant, the ratio of the apparent to the absolute permeability increases at t_2. Consequently by Equation (16), the pressure difference between experimental and calculated results increases with time.

The last observation might best be understood with the use of a relationship describing more accurately the actual or experimental flow. The Forchheimer [31] equation may be used, which is:

$$\alpha \mu q + \rho \beta q^2 = - \partial P/\partial X \qquad (18)$$

where $\alpha = 1/K$.

It may be noted from the above equation that with the second term of the left-hand side neglected, the result is simply Darcy's equation. Re-writing the equation, it becomes:

$$q = - (K/\mu)\ \partial P/\partial X\ - (1/\mu)\rho\beta K q^2 \qquad (19)$$

Again equating flow rates for the numerical and experimental data as before, the result becomes:

$$(\partial P/\partial x)_N = (K_{app}/K_{abs})\ (\partial P/\partial x)_E + (1-K_{app}/K_{abs})\rho\beta q^2 \qquad (20)$$

This last equation shows that neglecting the second term (quadratic in q), which was the case in this work, results in increasing difference between the numerical and experimental values with higher mean pressures. At high mean pressures K_{app} decreases and q increases.

These variations result in a decrease of the first term and increase in the absolute value of the second term of the right-hand side of the equation. The second term is always negative, K_{app} being

greater than K_{abs}. Therefore, the observation at high mean pressures, where the numerical and experimental values differ more, indicates that neglecting the second term in the evaluation of $(\partial P/\partial x)_N$ has a greater effect than the decrease in the (K_{app}/K_{abs}) factor of the first term.

CONCLUSIONS AND RECOMMENDATIONS

Primary Conclusion

The equipment as designed is capable of generating accurate data for analyzing pressure transient phenomena in gas flow through a linear porous system. In particular, it is capable of measuring instantaneous changes of pressure at time intervals as close as 0.6 seconds.

Secondary Conclusions

The validity of the flow tests performed on the equipment was well established. From the results of the tests and the observations made, the following conclusions were formulated:

1. The damage observed at both ends of the Berea Sandstone core may be due to two possibilities: namely, a) end effects, resulting from machining the core faces, and b) damage incurred in previous history of the core, unknown to this investigation. The apparent depth of this damage, as seen from the steady-state flow tests suggest the latter possibility to be the more probable cause.
2. Steady-state flow tests were found to describe adequately the permeability variation along a linear core, as well as delineations of turbulent flow regimes.
3. In pressure drawdown tests, the early stage of the transient is the most conducive to turbulent flow because it is when peak flow rates occur. However, flow rates at this period decline very sharply which suggests the temporary nature of the turbulent condition that may occur.
4. The rate of pressure buildup for the infinite reservoir case is greatest at the early period of the transient and then decreases as

it approaches the stabilized pressure. For low-permeability formations, the transient requires a very long time to attain stabilized conditions.

5. The transient tests apparently support the theory that, in a finite reservoir with an impervious boundary, once the transient reaches the boundary it assumes some definite patterns. These patterns may be described by a succession of steady-state conditions.
6. There is fair agreement between the numerical and experimental results for the studied case of pressure drawdown, infinite boundary. Deviations between the calculated and experimental values follow definite patterns: namely, a) the numerical solutions are generally lower, b) the magnitudes of their deviations increase (from zero at inlet) towards the outlet, with time of transient and with the initial imposed pressure.

Recommendations

The following suggestions may prove helpful in future studies of the same field as this investigation:

1. In the equipment used, control of boundary pressures may be improved by using supply valves and back-pressure regulators whose ranges are close to the experimental test range.
2. The mechanical-end-effect concept for explaining a damage as that observed in Cores 1 and 3, can be verified by re-cutting and machining the core at some point in the internal section, where steady-state flow tests indicated no damage. Then, steady-state flow tests will be run to check the damage.

If mechanical-end-effect was really a factor in this damage observed in the Berea and limestone cores, but not in the Alundum core, a good subject of investigation is a relation between this

end-effect and permeability. The Berea sandstone and limestone cores are low-permeability cores compared to the Alundum.

3. A closer agreement between the unsteady-state experimental results and the numerical results may be attained by: using the relationship of apparent permeability instead of the absolute permeability; and applying Equation 5, which was proposed by Green and Duwez [19], instead of Darcy's Equation. The use of these two relationships, however, is much more involved.

NOMENCLATURE

A	-	cross-sectional area, square feet
β	-	inertial resistance coefficient
c	-	reservoir compressibility, Vols/vol/psi
Δ	-	difference or change
h	-	net pay, feet
K	-	permeability, millidarcy
L	-	length, feet
M	-	molecular weight of gas
ϕ	-	pososity
P	-	pressure, psi
$\underline{P}$	-	dimensionless pressure
Pm	-	mean pressure, psi
q	-	volumetric flow rate per unit area, $Ft^3/Sec/Ft^2$
R	-	universal gas constant
r	-	radial distance from well, feet
ρ	-	gas density
t	-	time, hours
$\underline{t}$	-	dimensionless time
T	-	absolute temperature, ^oF
μ	-	viscosity, cps
x	-	horizontal distance
$\underline{x}$	-	dimensionless distance
Z	-	compressibility factor of gas

Subscripts:

abs	-	absolute
app	-	apparent
e	-	external boundary
i,j,k,	-	grid coordinates
n	-	time steps
0	-	at initial time
S	-	static condition
w	-	wellhead

BIBLIOGRAPHY

1. Muskat, M. "Use of Data on the Buildup of Bottomhole Pressure", Trans. AIME, Vo. 123, 1937, P. 44.

2. Horner, D.R. "Pressure Buildup in Wells", Proc. of the Third World Petroleum Congress, Section 11, 1951, P. 503.

3. Miller, C.C., Dyes, A.B. and Hutchinson C.A. Jr., "The Estimation of Permeability and Reservoir Pressure from Bottom-Hole Pressure Buildup Characteristics", Trans, AIME, Vo. 189, 1950, P. 91.

4. Thomas, G.B. "Analysis of Pressure Buildup Data", Trans AIME, Vo. 198, 1953, P. 125.

5. Van Everdingen, A.F. "The Skin Effect and Its Influence on the Production Capacity of A Well", Trans. AIME, Vo. 198, 1953, P. 171.

6. Hurst, W. "Establishment of the Skin Effect and Its Impediment to Fluid Flow into the Well-bore", Petroleum Engineer, Oct., 1953, P. B-6.

7. Arps, J.J. "How Well Completion Damage can be Determined Rapidly", World Oil, April, 1955, P. 225.

8. Gladfeller, R.E., Tracy, G.W., and Wilsey, L.E., "Slecting Wells Which Will Respond to Production Stimulation Treatment", API Drilling and Production Practices, 1955, P. 117.

9. Perrine, R.R. "Analysis of Pressure Buildup Curves", API Drilling and Production Practices, 1964, P. 115.

10. Landrum, B.L. and Flanagan, D.A. "A New Experimental Model for Studying Transient Phenomena", Trans. AIME, Vo. 216, 1959, P. 33.

11. Goodknight, R.C., Klinkoff, W.A., Jr. and Falt, I. "Non-Steady State Fluid Flow and Diffusion in Porous Media Containing Dead-End Pore Volume", J. Phys. Chem., Vo. 64, No. 9, 1960, P. 1162.

12. Bruce, G.H., Peaceman, D.W. and Rachford, H.H. "Calculations of Unsteady-State Gas Flow Through Porous Media", Trans. AIME, Vo. 198, 1953, P. 79.

13. Van Everdingen, A.F. and Hurst W. "The Application of the Laplace Transformation to Flow Problems in Reservoirs", Trans. AIME, Vo. 186, 1949, P. 305.

14. Katz et al, "Handbook of Natural Gas Engineering", McGraw-Hill, 1959.

15. Flock, D.L. and Aziz K. "Unsteady-State Gas Flow - Use of Drawdown Data in the Prediction of Gas Well Behavior", Reprint from the Journal of Canadian Petroleum Technology, Vo. 2, No. 1, Spring, 1963.

16. Jenkins, R. and Aronofsky, J.S. "Unsteady Radial Flow of Gas Through Porous Media", ASME Applied Mechanics Division, June, 1953, P. 210.

17. Collins, R.E. and Crawford, P.B. "Calculations of Unsteady-State Gas Flow Through Porous Media, Corrected for Klinkenberg Effect", Trans. AIME, Vo. 198, 1953, P. 339.

18. Jones, L.G. "An Approximate Method of Computing Non-Steady-State Flow of Gases in Porous Media", Trans, AIME, Vo. 222, 1961, P. II-264.

19. Green, L. and Duwez, P. "Fluid Flow Through Porous Metals" Journal of Applied Mechanics, Vo. 186, 1951, P. 36.

20. Aronofsky, J.S. and Jenkins, R. "A Simplified Analysis of Unsteady Radial Gas Flow", Trans. AIME, Vo. 201, 1954, P. 149.

21. Klinkenberg, L.J. "The Permeability of Porous Media to Liquids and Gas", API Drilling and Production Practices, 1941. P. 200.

22. Hirschfelder, J.O., Curtiss, C.F. and Bird R.B. "Molecular Theory of Gases and Liquids", John Wiley and Sons, 1954, P. 15.

23. Hilsenrath, J., Becket, C.W., Benedict, W.S., Fano, L., Hoge, H.J., Masi, J.F., Touloukian, Y.S., and Wooley, H.W. "Tables of Thermal Properties of Gases", National Bureau of Standard,
24. Washington, D.C. Circular 554, Table 7-1, 1955, P. 317.

24. Kestin, J. and Wang, H.E. "The Viscosity of Five Gases: A Re-Evaluation", Trans. AIME, Table 1, Vo. 80, 1959, P. 13.

25. Hamilton, R.J. "A Study of Linear, Steady-State, Gas Flow Through Consolidated Porous Media", Master's Thesis in Petroleum Engineering, University of Alberta, Feb. 1963.

26. Mackett, R.A. "Viscous and Visco-Inertial Gas Flow in Limestone Cores", Master's Thesis in Petroleum Engineering, University of Alberta, 1966.

27. Dranchuk, P.M. and Sadiq, S. "The Interpretation of Permeability Measurements", Reprint from the Journal of Canadian Petroleum Technology, Fall, 1965.

28. Sadiq, S. "Inertial Resistance Coefficient and Rock Properties", Master's Thesis in Petroleum Engineering, University of Alberta, 1965.

29. Wilson, L.H., Sibbit, W.L. and Jakob, M. "Flow of Gases in Porous Media", J. of Applied Physics, Vo. 22 #8, Aug. 1951, P. 1027.

30. Pitzer, S.C. "Uses of Transient Pressure Tests", API Drilling and Production Practices, 1964. P. 115.

31. Forchheimer, P. "Wassenbewegun Durch Boden", Zeitschrift des Vereines Deutscher Ingenieure, Vol. 45, 1901, P. 1782.

32. Kolada, L.V. "Steady Linear Gas Flow Through Porous Media", Master's Thesis in Petroleum Engineering, University of Alberta, 1968.

33. Calhoun, J.C., Jr. "Fundamentals of Reservoir Engineering", University of Oklahoma Press., 1953.

34. Mungan, N. "Permeability Reduction Through Changes in PH and Salinity", Trans, AIME, Vol. 234, 1965, P. 1449.

APPENDIX I

GRAPHICAL RESULTS

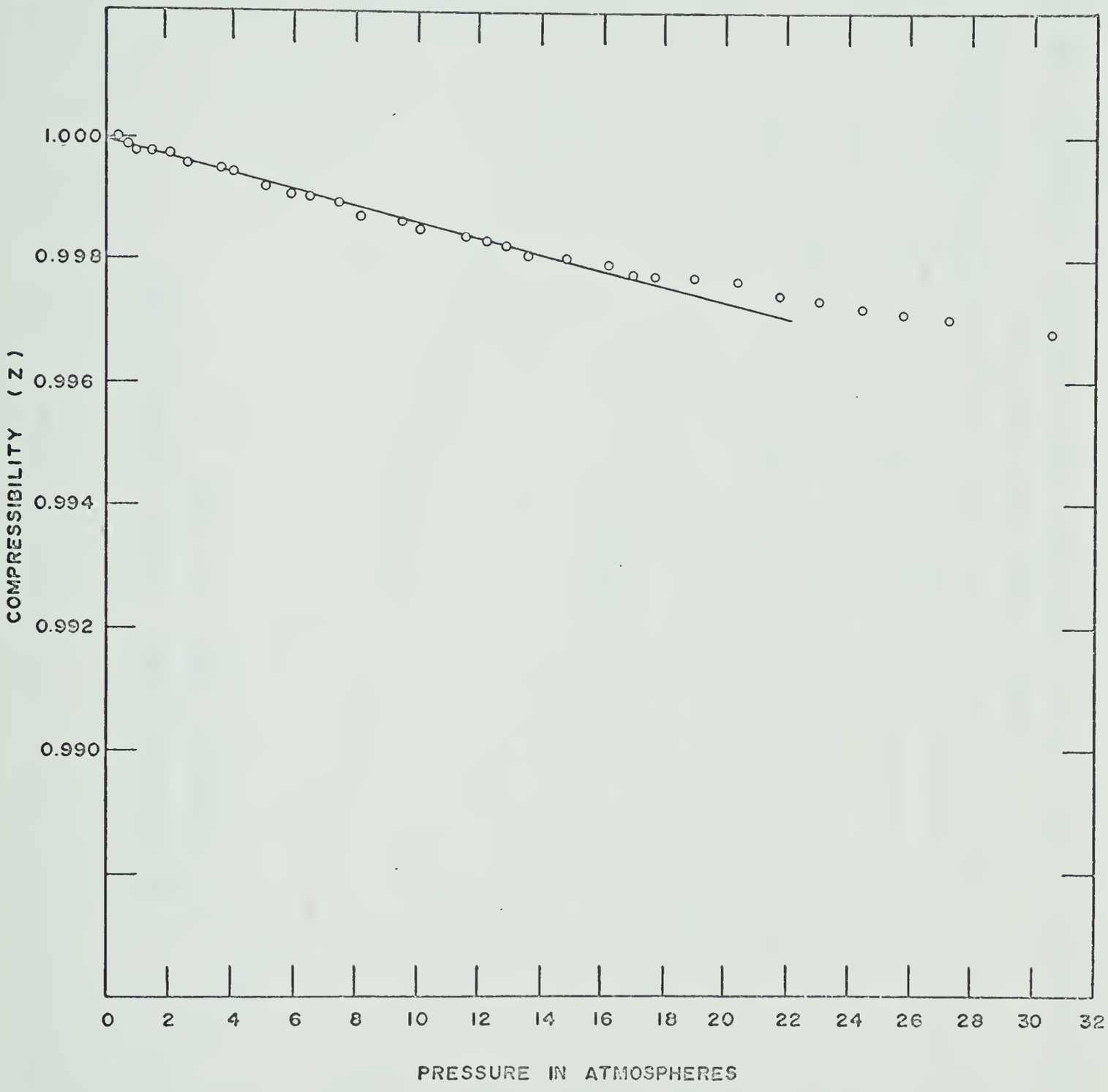

Figure 1A. COMPRESSIBILITY OF NITROGEN AS FUNCTION OF PRESSURE INTERPOLATED FOR TEMPERATURE OF 78° F

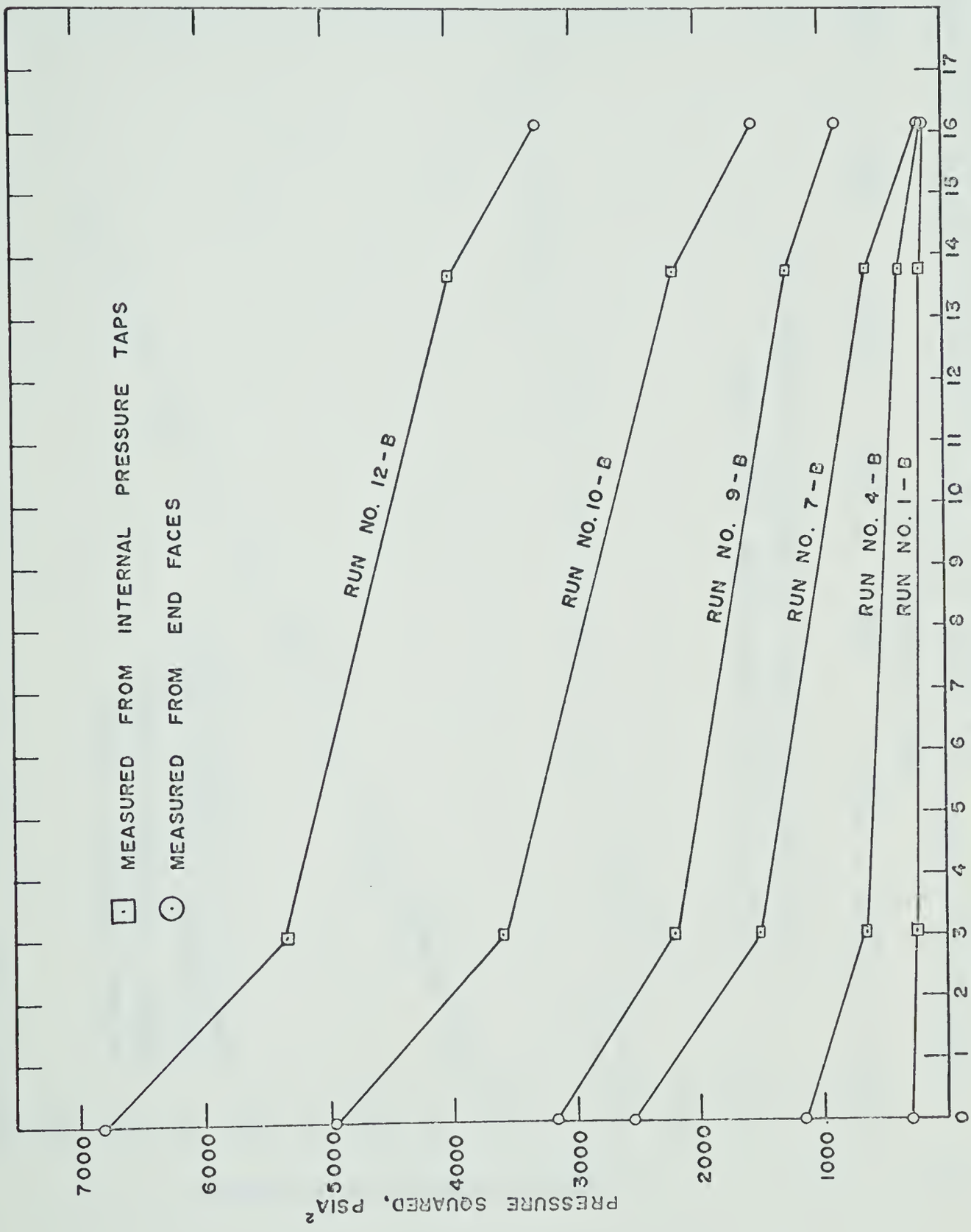

Figure 2A. STEADY FLOW TESTS ON LIMESTONE, CORE 3, VERIFYING MECHANICAL END EFFECTS

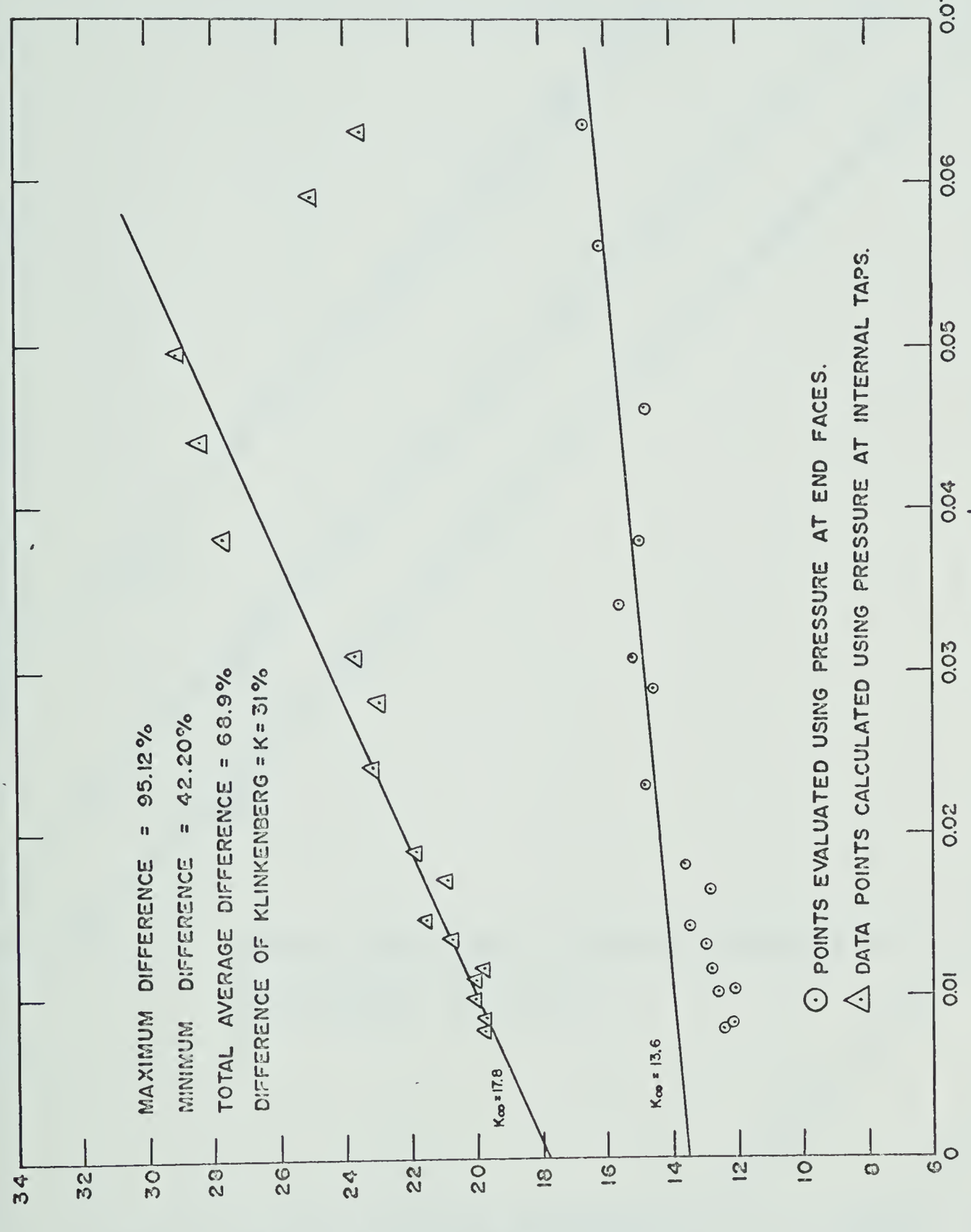

Figure 3A. STEADY FLOW TESTS, SHOWING DIFFERENCE IN CALCULATED APPARENT PERMEABILITIES WHEN PRESSURES ARE MEASURED AT (1) MACHINED FACES OF TIGHT CORE, (2) INSIDE OF CORE 3

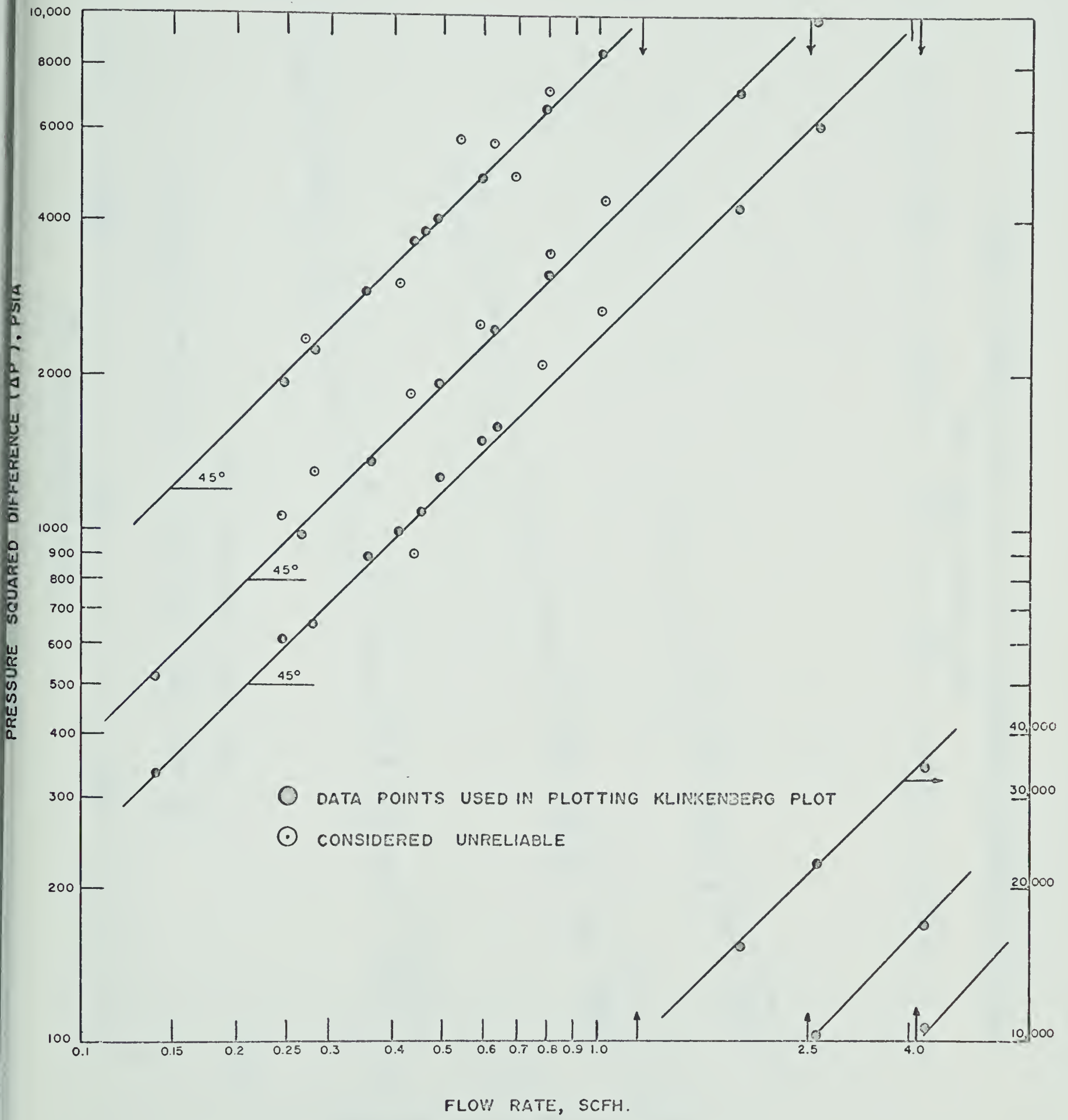

Figure 4A. FLOW REGIME PLOT OF CORE I.

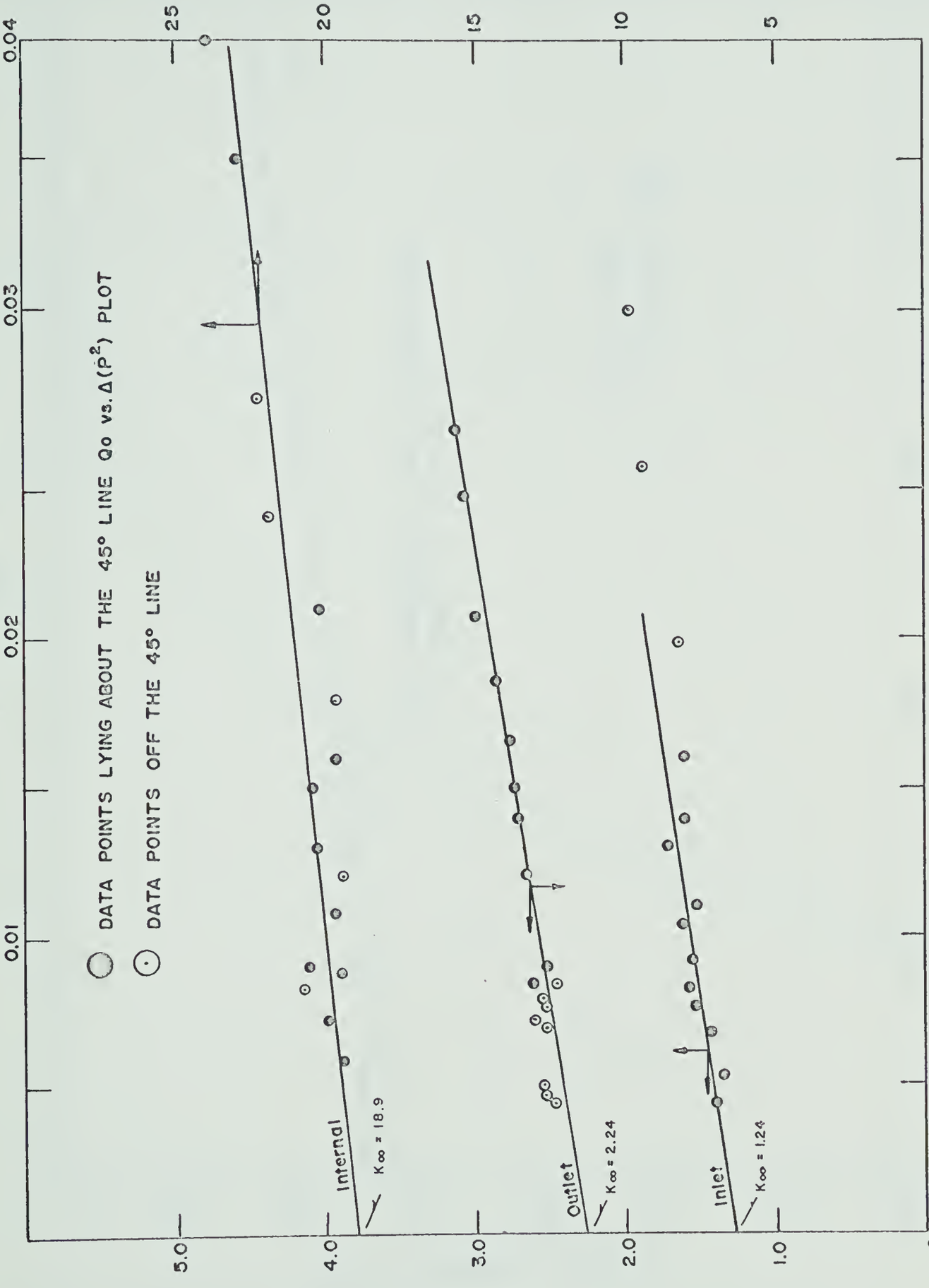

Figure 5A. KLINKENBERG PERMEABILITY PLOT FOR THREE SECTIONS OF CORE I.

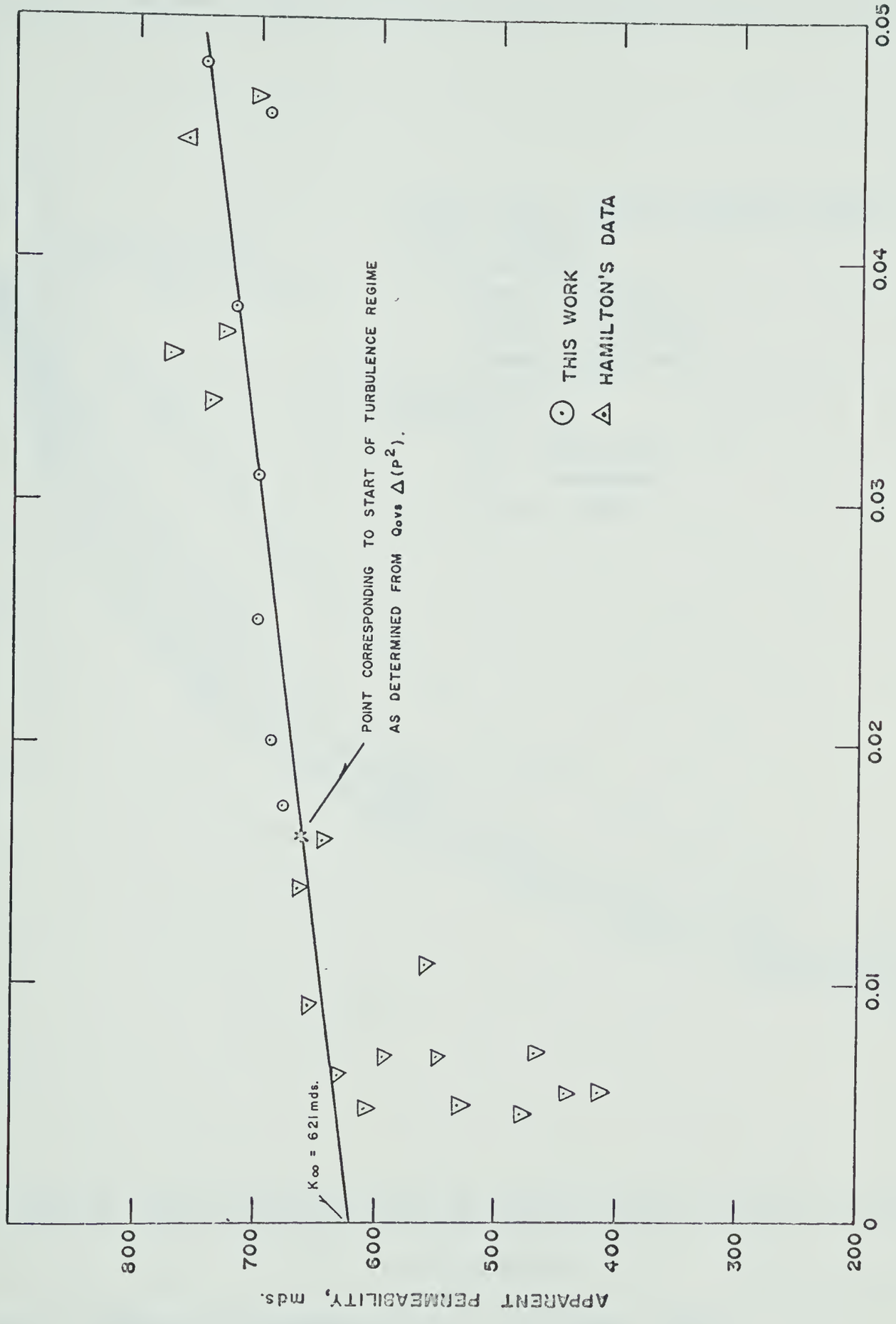

Figure 6A. KLINKENBERG PERMEABILITY PLOT OF THE ALUNDUM CORE (CORE 2).

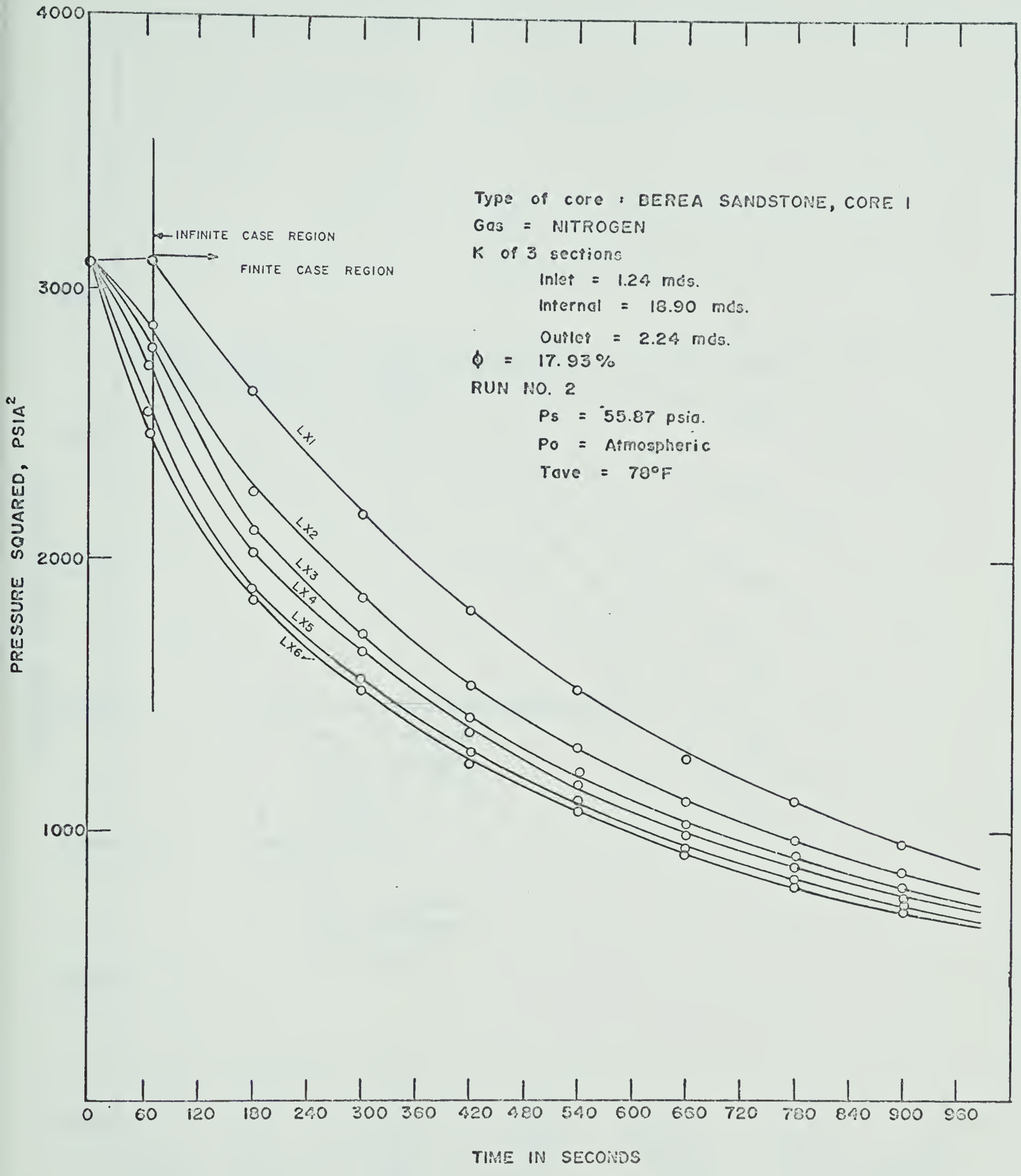

Figure 7A. PRESSURE DRAWDOWN, P^2 vs. T, NO INFLUX CASE.

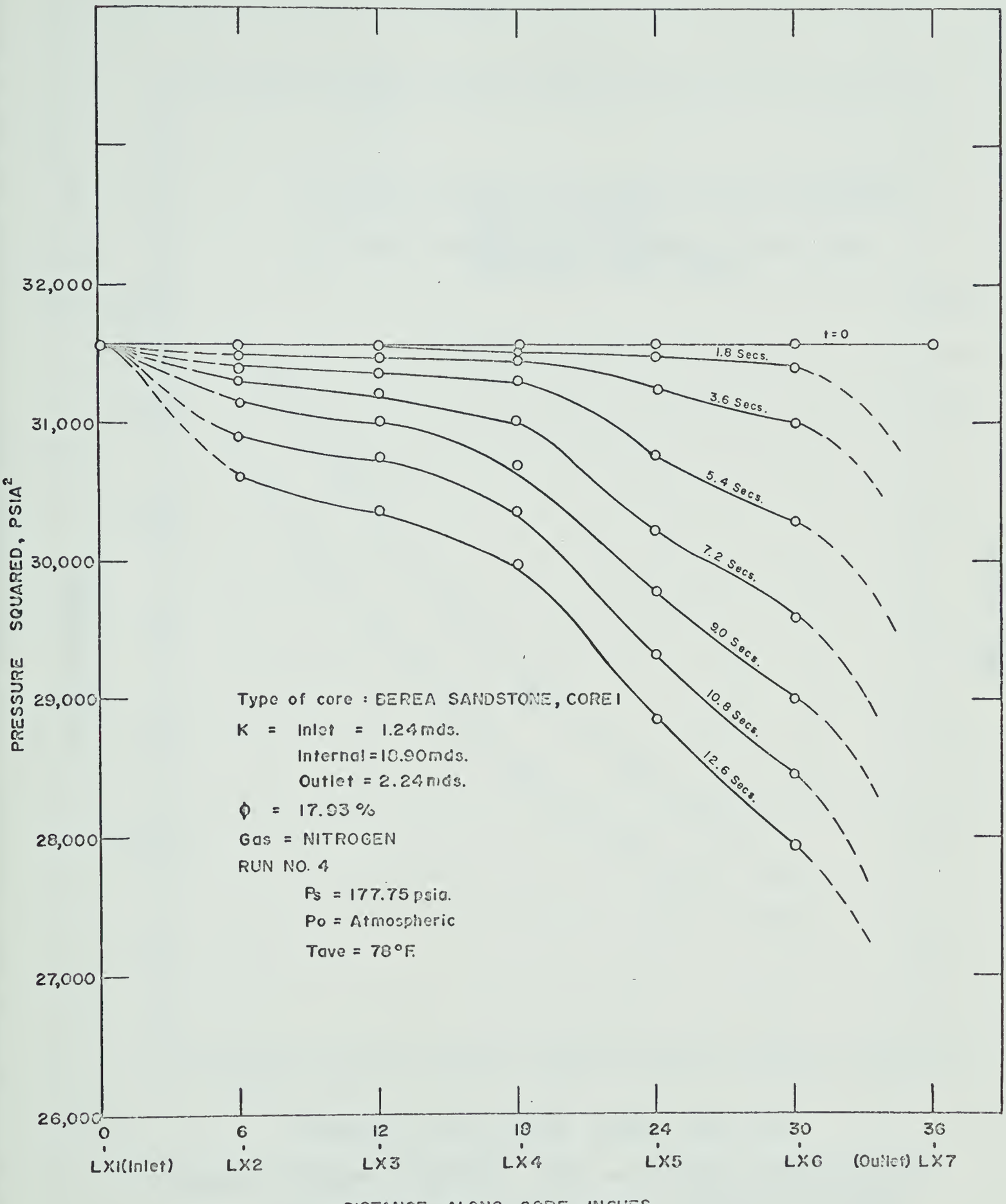

Figure 8A. PRESSURE DRAWDOWN, P^2 vs X, TAKEN BEFORE RESPONSE WAS OBSERVED AT INLET FROM NO-INFLUX CASE.

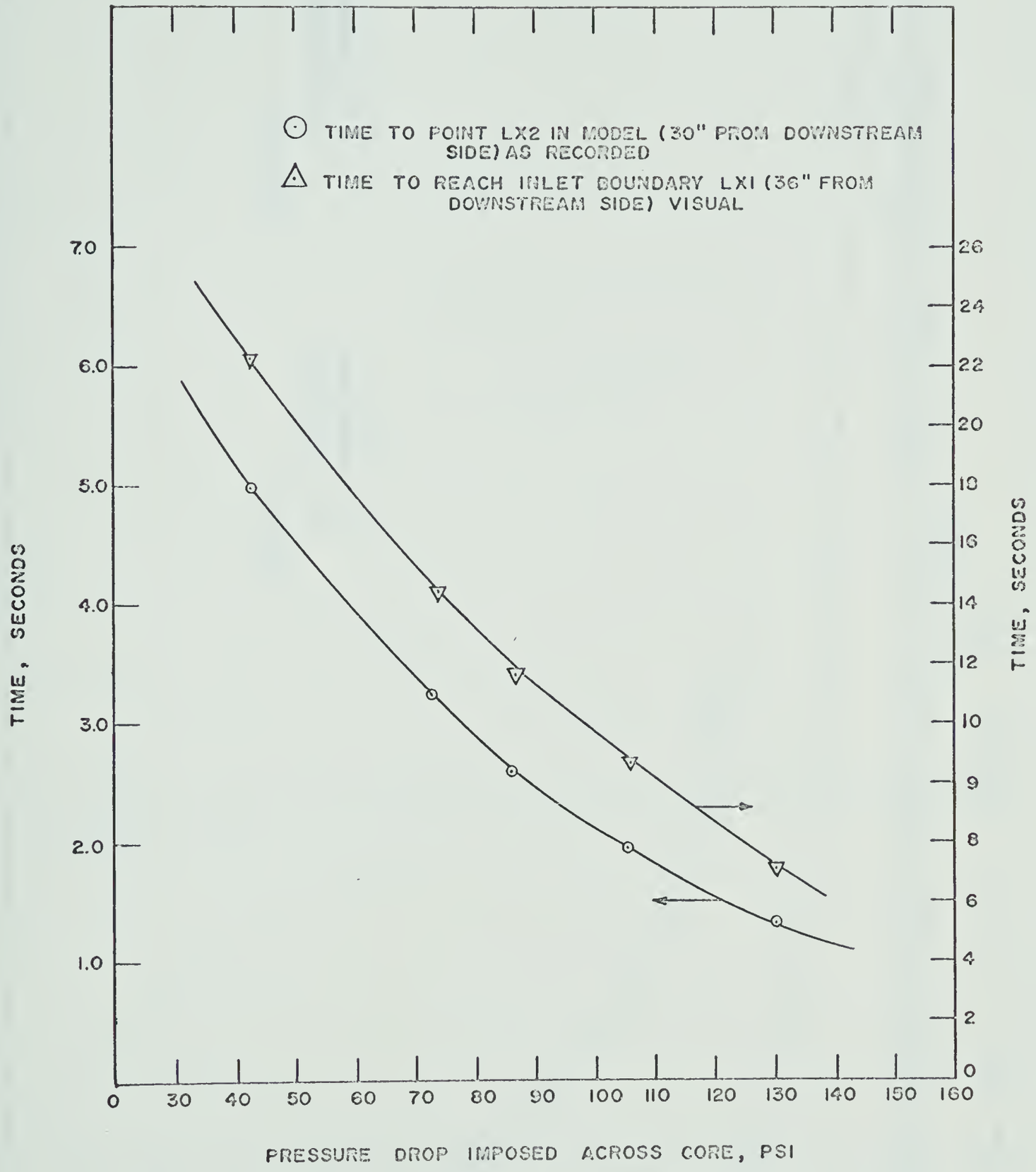

Figure 9A. PRESSURE TRANSIENT TIME vs. IMPOSED PRESSURED DROP FOR CORE I, PRESSURE DRAWDOWN CONSTANT PRESSURE OUTLET CASE

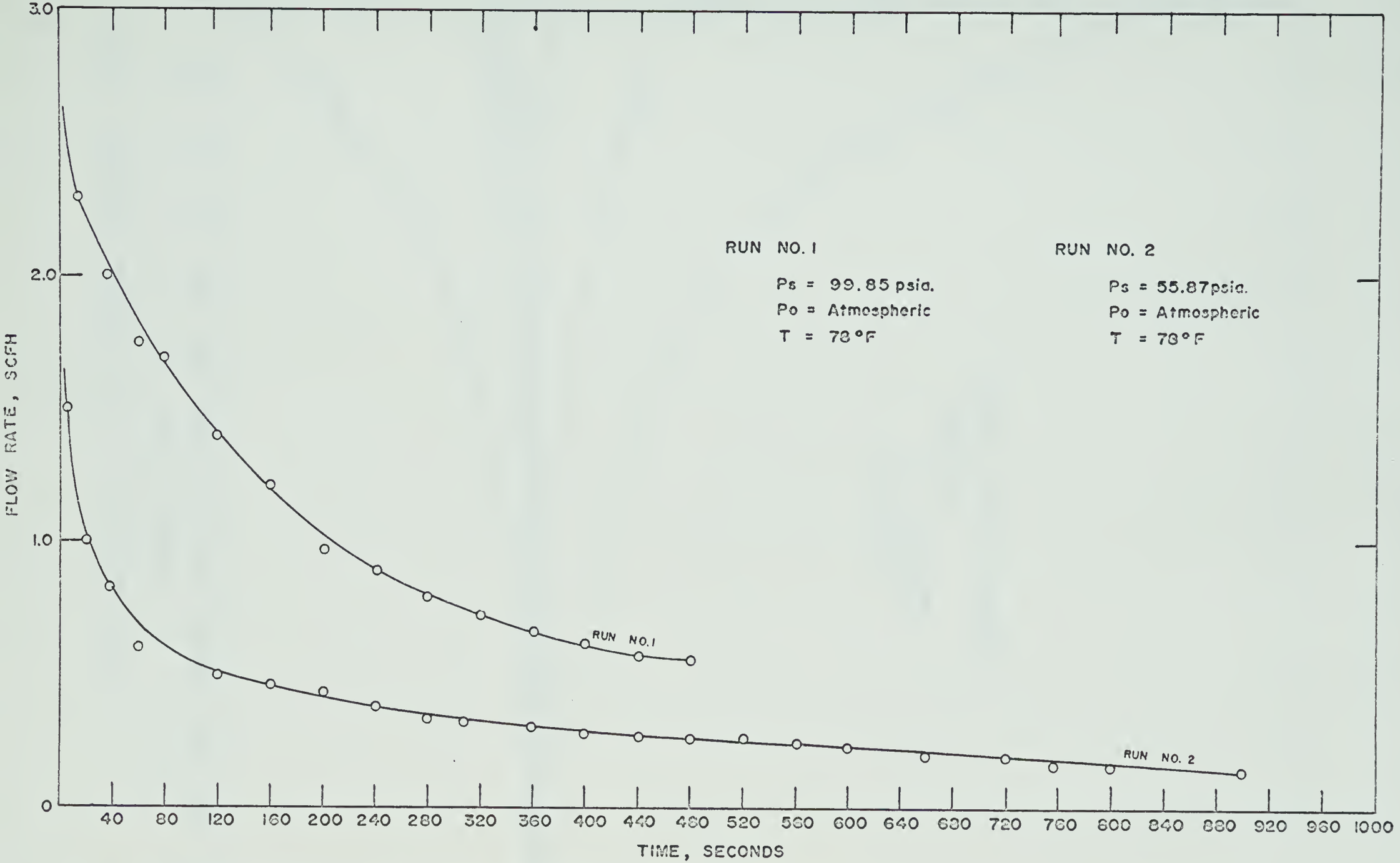

Figure 10A. FLOW RATE vs. TIME OF TRANSIENT, CORE 1.

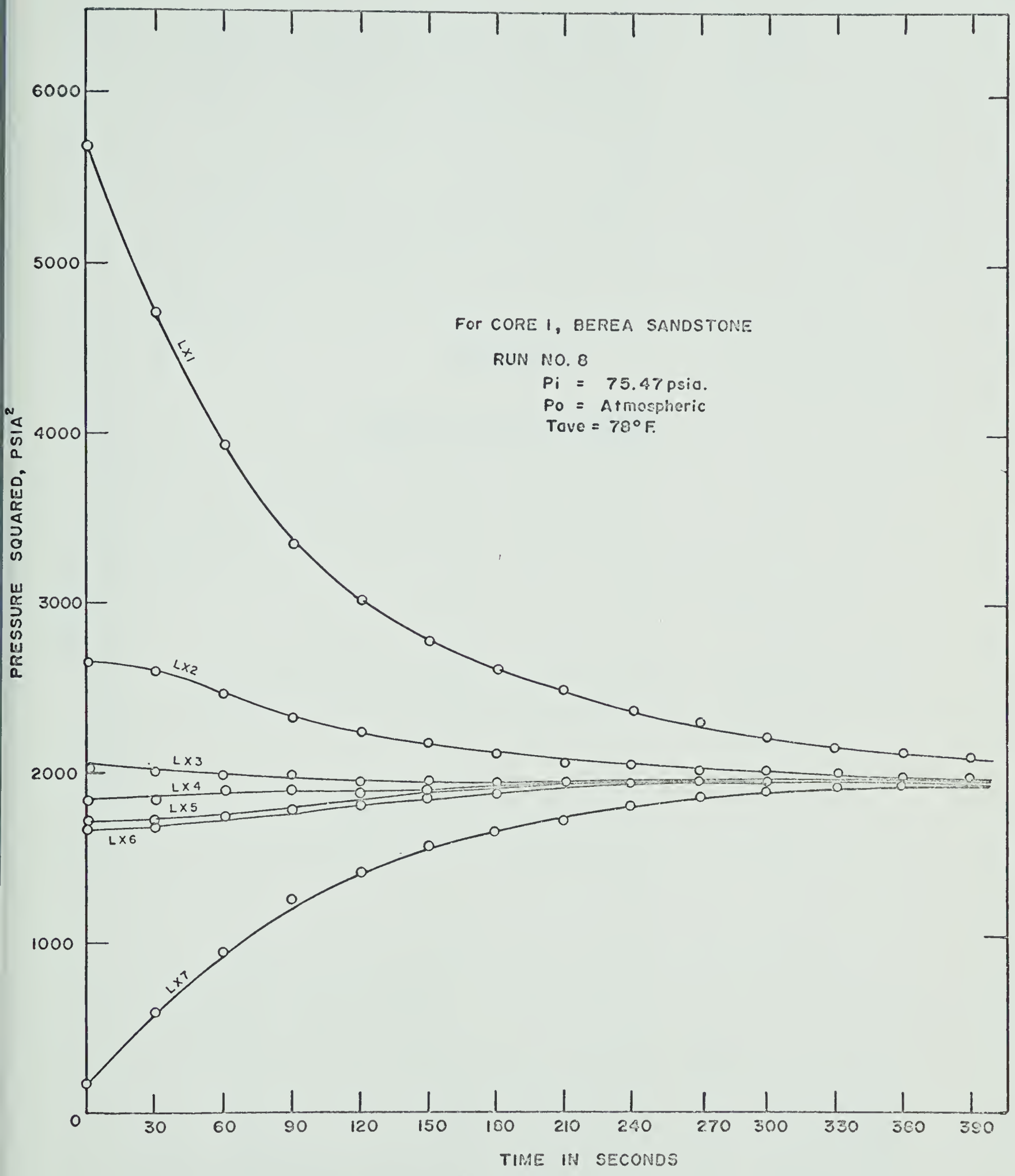

Figure IIA. PRESSURE BUILDUP, P^2 vs. T, NO INFLUX, CASE.

APPENDIX II

TABLES OF DATA AND RESULTS

TABLE 1A

Porosity Data and Calculations for the Berea Sandstone and Alundum Cores

DATA:

Sample	Average Length (inches)	Average Diameter (inches)	Bulk Volume (cc)	Source tank pressure before opening valve (psia)	Expansion chamber press. before opening valve ("Hg.vac)	equalized pressure (psia)
Calibration blanks						
Empty	-	-	0	213.69	27.92	35.09
# 1	0.509	0.747	3.671	213.69	27.92	34.19
# 2	0.627	0.747	4.522	213.69	27.92	33.95
# 3	0.799	0.748	5.768	213.69	27.92	33.49
# 4	1.036	0.749	7.472	213.69	27.92	32.99
# 5	1.308	0.748	9.422	213.69	27.92	32.44
# 1&5	-	-	13.093	213.69	27.92	31.39
# 1,4&5	-	-	20.565	213.69	27.92	30.19
berea # 1	1.319	1.004	17.11	213.69	27.92	31.19
berea # 2	1.147	1.005	14.91	213.69	27.92	31.59
berea # 3	0.887	1.008	11.60	213.69	27.92	32.39
alundum #4	0.793	1.01	10.41	213.69	27.92	32.99
alundum #5	0.744	1.000	9.58	213.69	27.92	33.16

CALCULATIONS:

Core Samples	Grain Vol. from Calibration graph(cc)	Porosity (%)	Average Porosity (%)
berea # 1	14.0 cc	18.18	
berea # 2	12.5 cc	17.50	17.93
berea # 3	9.5	18.10	
alundum # 4	7.4	28.88	28.91
alundum # 5	6.81	28.95	

TABLE $2A_1$
STEADY STATE FLOW - PRESSURE DISTRIBUTION
CORE 1 BEREA SANDSTONE

Run No.	Q (SCFH)	T(Ave) ^oR	Pressure squared - psia^2						
			P_1^2	P_2^2	P_3^2	P_4^2	P_5^2	P_6^2	P_7^2
1	0.10	538.0	1397.3	747.5	615.5	571.2	540.1	532.7	192.7
2	0.14	538.0	2050.3	1034.3	830.6	761.8	717.7	703.3	192.7
3	0.27	538.0	3841.5	1498.5	1383.8	1273.8	1191.6	1169.6	192.7
4	0.35	538.1	5340.7	2443.3	1863.7	1705.7	1586.0	1552.4	192.7
5	0.49	538.1	7418.4	3365.2	2540.2	2322.3	2162.3	2112.3	192.7
6	0.62	538.1	9926.1	4305.9	3221.7	2949.6	2745.8	2674.9	192.7
7	0.79	538.1	11517.1	5484.9	4070.4	3728.3	3472.7	3377.9	192.7
8	0.24	538.2	6724.0	4812.2	4436.9	4316.5	4239.3	4204.2	3124.8
9	0.44	537.8	9604.0	5929.0	5422.8	5222.9	5090.8	5032.5	3169.7
10	0.59	537.9	11990.3	7226.7	6267.9	5993.8	5818.6	5736.5	3209.2
11	0.80	538.0	15400.8	8766.6	7399.4	7040.9	6799.7	6699.7	3237.6
12	1.03	537.9	18933.8	10391.6	8621.1	8159.5	7844.6	7701.8	3260.4
13	0.28	538.0	10739.2	8508.6	8085.6	7956.5	7878.3	7849.9	5116.5
14	0.38	538.0	14781.7	10308.3	9426.5	9181.5	9030.7	8979.5	5130.8
15	0.53	538.1	18782.7	12968.6	11791.8	11481.1	11274.2	11193.6	8172.2
16	0.69	538.0	18782.7	13947.6	12991.4	12582.1	12582.1	12521.6	10020.0
17	0.45	537.9	18763.5	14957.3	14230.1	14069.9	13921.6	13876.8	11854.8
18	0.41	538.0	18763.5	15760.3	15101.9	14925.5	14801.6	14762.5	12550.7
19	4.41	538.0	69326.9	35310.6	31420.7	30614.8	28015.6	24610.4	7610.4
20	2.77	538.1	44753.4	22563.2	20303.2	18453.2	16953.1	16463.8	6453.3
21	1.90	538.0	29894.4	14835.5	13212.6	12215.7	11926.8	10626.6	3507.4

TABLE $2A_2$
STEADY STATE FLOW - PRESSURE DISTRIBUTION
CORE 2 ALUNDUM

Run No.	Q (SCFH)	T(Ave) ^{o}R	Pressure squared - psia^2						
			P_1^2	P_2^2	P_3^2	P_4^2	P_5^2	P_6^2	P_7^2
1	2.48	537.9	580.3	552.2	478.3	407.6	341.1	275.8	181.9
2	4.25	537.8	894.0	813.9	691.6	576.0	463.1	359.4	182.2
3	1.10	537.9	300.6	278.8	260.1	241.1	223.8	207.9	192.9
4	1.60	538.0	451.1	407.2	262.1	317.9	279.2	244.3	222.7
5	3.21	538.0	723.0	647.7	556.4	468.7	386.1	310.4	226.2
6	6.00	538.0	1252.4	1098.2	925.9	764.5	603.6	459.6	290.3
7	9.03	538.1	1904.4	1631.3	1369.7	1125.6	882.0	662.0	409.6
8	13.52	538.1	2904.1	2506.0	2113.2	1744.7	1373.4	1042.0	672.8
9	18.76	538.1	4275.8	3654.2	3105.8	2593.8	2075.7	1613.2	1114.8
10	23.36	538.0	5646.0	4846.9	4152.5	3499.9	2846.2	2262.9	1635.4

TABLE 3A
GAS FLOW DATA
CORE 3 LIMESTONE

Run # B	Q (SCFH)	T(Ave) ^{o}R	P_i^2 (inlet face) $psia^2$	P_1^2 (internal) $psia^2$	P_2^2 (internal) $psia^2$	P_o^2 (outlet face) $psia^2$	Ka (internal) mds.	Ka (external) mds.
1	0.20	538.1	329.8	282.9	214.9	181.2	16.7	23.4
2	0.43	538.0	499.9	362.1	226.8	181.2	16.2	24.5
3	0.81	538.0	862.0	537.3	313.3	186.6	14.9	29.2
4	1.25	538.0	1146.5	690.1	363.3	189.3	15.1	28.4
5	1.67	538.2	1525.7	977.8	433.5	192.1	15.6	24.6
6	2.21	538.1	2002.6	1144.5	516.6	194.9	15.3	28.2
7	2.74	537.8	2514.0	1538.2	615.0	201.4	14.8	23.7
8	3.39	537.8	3213.8	1923.7	739.8	214.3	14.1	22.9
9	2.72	537.9	3162.9	2228.8	1290.2	878.5	14.8	23.2
10	3.79	538.0	4995.7	3564.0	2181.8	1546.9	13.7	21.9
11	5.31	538.0	6761.8	4565.7	2534.1	1598.4	12.8	20.9
12	3.78	538.0	6811.2	5364.1	3962.7	3321.2	13.6	21.5
13	6.29	538.0	9645.6	6945.6	4522.5	3520.0	12.8	20.7
14	4.37	538.1	9688.4	7967.3	6218.9	5436.1	12.8	19.9
15	7.20	538.1	12923.1	9718.0	6852.5	5502.6	12.1	20.0
16	4.92	538.0	12977.8	10997.7	9074.5	8103.6	12.5	20.4
17	4.70	538.0	17561.5	13486.2	9900.3	8230.1	12.3	20.6
18	6.68	538.0	18884.2	16025.0	13344.9	12016.5	12.1	19.8
19	6.06	538.0	18955.8	16489.1	14118.2	12911.8	12.5	19.9

TABLE 4A
GAS FLOW DATA
CORE I BEREA SANDSTONE

INLET SECTION

Run No.	Tave ^{o}R	Q (SCFH)	$P_1^2-P_2^2$ $(psia)^2$	1/Pm $(psia^{-1})$	K_{app} (mds)
1	538.1	0.10	649.8	0.0310	1.96
2	538.2	0.14	1016.0	0.0258	1.86
3	538.2	0.27	2343.1	0.0199	1.63
4	538.2	0.35	2897.3	0.0163	1.59
5	538.2	0.49	4053.2	0.0139	1.57
6	538.3	0.62	5620.2	0.0121	1.44
7	538.3	0.79	7032.3	0.0107	1.47
8	538.4	0.24	1911.8	0.0132	1.66
9	537.9	0.44	3675.0	0.0114	1.55
10	538.0	0.59	4763.6	0.0103	1.61
11	538.0	0.80	6634.2	0.0092	1.56
12	538.0	1.03	8542.0	0.0083	1.56
13	538.1	0.28	2230.9	0.0102	1.65
14	538.1	0.38	4473.4	0.0089	1.54
15	538.2	0.53	5814.1	0.0090	1.56
16	538.1	0.69	4835.1	0.0078	1.56
17	538.6	0.45	3806.2	0.0077	1.55
18	538.2	0.41	3003.2	0.0076	1.78
19	538.1	4.41	34016.2	0.0044	1.41
20	538.2	2.77	22190.2	0.0055	1.35
21	538.1	1.90	15058.9	0.0068	1.44

INTERNAL SECTION

Run No.	Tave ^{o}R	Q (SCFH)	$P_2^2-P_6^2$ $(psia)^2$	1/Pm $(psia^{-1})$	K_{app} (mds)
1	538.0	0.10	214.8	0.040	23.81
2	538.0	0.14	330.9	0.036	22.88
3	538.0	0.27	328.8	0.028	22.10
4	538.1	0.35	890.9	0.024	21.90
5	538.1	0.49	1252.8	0.021	20.41
6	538.1	0.62	1631.0	0.018	19.95
7	538.1	0.79	2106.9	0.016	19.70
8	538.2	0.24	607.9	0.015	20.64
9	537.8	0.44	897.0	0.014	20.71
10	537.9	0.59	1490.2	0.013	20.63
11	538.0	0.80	2068.8	0.012	20.06

TABLE 4A - continued

INTERNAL SECTION - continued

Run No.	Tave ^{o}R	Q (SCFH)	$P_2^2-P_6^2$ $(psia)^2$	1/Pm $(Psia^{-1})$	K_{app} (mds)
12	537.9	1.03	2689.9	0.011	19.90
13	538.0	0.28	658.3	0.011	22.40
14	538.0	0.38	1328.8	0.010	20.84
15	538.1	0.53	1775.1	0.009	20.54
16	538.0	0.69	1426.0	0.009	21.92
17	537.9	0.45	1080.4	0.009	21.95
18	538.0	0.41	998.0	0.008	21.49
19	538.0	4.41	10700.2	0.006	19.57
20	538.1	2.77	6119.0	0.007	20.00
21	538.0	1.90	4209.9	0.009	19.67

OUTLET SECTION

Run No.	Tave ^{o}R	Q (SCFH)	$P_6^2-P_7^2$ $(psia)^2$	1/Pm $(psia^{-1})$	K_{app} (mds)
1	537.9	0.10	340.0	0.054	3.13
2	537.8	0.14	510.6	0.049	3.09
3	537.8	0.27	976.9	0.041	2.97
4	538.0	0.35	1359.7	0.038	2.83
5	538.0	0.49	1919.7	0.033	2.77
6	537.9	0.62	2482.3	0.030	2.73
7	537.9	0.79	3185.3	0.028	2.71
8	538.0	0.24	1097.4	0.017	2.46
9	537.7	0.44	1862.8	0.016	2.55
10	537.8	0.59	2527.4	0.015	2.53
11	538.0	0.80	3460.2	0.014	2.49
12	537.8	1.03	4441.4	0.014	2.51
13	537.9	0.28	2733.5	0.013	1.75
14	537.9	0.38	3848.7	0.012	1.66
15	538.0	0.53	3021.4	0.010	2.51
16	537.9	0.69	2501.6	0.009	2.52
17	537.8	0.45	2021.9	0.009	2.43
18	537.8	0.41	2211.5	0.008	2.02
19	537.9	4.41	17000.0	0.008	2.59
20	538.0	2.77	10009.5	0.009	2.52
21	537.9	1.90	7119.2	0.012	2.63

TABLE 5A
GAS FLOW DATA
CORE 2 ALUNDUM

Run No.	Tave ^{o}R	Q (SCFH)	$P_1^2-P_7^2$ $(psia)^2$	1/Pm $(psia^{-1})$	K_{app} (mds)
1	537.8	2.48	398.4	0.053	720.5
2	537.8	4.25	711.8	0.046	690.9
3	538.0	1.10	107.8	0.064	694.9
4	538.0	1.60	248.4	0.056	745.7
5	538.1	3.21	496.9	0.048	747.5
6	538.1	6.00	962.1	0.038	721.7
7	538.1	9.03	1494.8	0.031	699.0
8	538.0	13.52	2231.3	0.025	701.1
9	538.1	18.76	3160.9	0.020	686.7
10	538.0	23.36	4010.6	0.017	673.9

TABLE 6A
COMPUTER OUTPUT
EXPERIMENTAL DRAWDOWN

RUN NO. 1, CORE 1

INFINITE BOUNDARY CASE

TIME SEC.	LX1 PSQR	LX2 PSQR	LX3 PSQR	LX4 PSQR	LX5 PSQR	LX6 PSQR	LX7 PSQR
0	9930.7	9930.7	9930.7	9930.7	9930.7	9930.7	9930.7
3.6	9930.7	9930.7	9930.7	9930.7	9904.4	9850.7	183.6
7.2	9930.7	9921.5	9921.5	9907.2	9767.5	9613.9	183.6
10.8	9930.7	9888.5	9888.5	9840.8	9559.1	9349.1	183.6
14.4	9930.7	9804.1	9781.4	9686.7	9300.8	9042.3	183.6
18.0	9930.7	9714.2	9659.9	9537.6	9091.8	8830.5	183.6
21.6	9930.7	9680.4	9590.9	9430.9	8941.8	8865.9	183.6
25.2	9930.7	9590.1	9455.4	9269.6	8751.8	8473.4	183.6

FINITE BOUNDARY CASE

25.2	9930.7	9590.1	9455.4	9269.6	8741.8	8473.4	183.6
55.0	9712.3	8742.3	8338.4	8073.2	7567.4	7308.7	183.6
80.0	9322.1	8037.9	7550.7	7277.9	6816.3	6575.7	183.6
105.0	8565.7	7435.6	6940.4	6671.1	6253.8	6042.1	183.6
150.0	7841.3	6493.1	5988.1	5741.8	5378.5	5191.3	183.6
203.0	6814.6	5562.6	5118.9	4891.4	4576.6	4415.7	183.6
381.0	4296.9	3496.7	3214.3	3074.4	2875.2	2776.3	183.6

TABLE 6A-CONTINUED

RUN NO. 2, CORE 1

INFINITE BOUNDARY CASE

TIME SEC.	LX1 PSQR	LX2 PSQR	LX3 PSQR	LX4 PSQR	LX5 PSQR	LX6 PSQR	LX7 PSQR
0.0	3121.8	3121.8	3121.8	3121.8	3121.8	3121.8	3121.8
6.0	3121.8	3116.7	3116.7	3116.2	3101.7	3094.9	186.9
12.0	3121.8	3101.7	3101.7	3101.7	3067.2	3024.2	186.9
18.0	3121.8	3098.6	3098.5	3087.9	2995.7	2936.8	186.9
24.0	3121.8	3083.5	3075.9	3054.6	2927.1	2859.3	186.9
30.0	3121.8	3056.3	3043.6	3009.3	2861.5	2791.3	186.9
36.0	3121.8	3030.0	3007.3	2960.1	2801.9	2732.4	186.9
42.0	3121.8	3016.2	2983.4	2931.2	2757.6	2682.5	186.9
48.0	3121.8	2981.9	2934.5	2882.7	2710.5	2632.9	186.9
54.0	3121.8	2943.9	2886.8	2825.2	2652.5	2575.8	186.9
60.0	3121.8	2911.5	2842.5	2771.2	2600.3	2527.3	186.9
FINITE BOUNDARY CASE							
63.0	3121.7	2909.8	2835.8	2759.7	2589.0	2519.3	186.9
180.0	2618.6	2295.1	2154.1	2072.5	1942.4	1889.9	186.9
300.0	2169.0	1908.5	1774.3	1704.3	1597.0	1551.8	186.9
420.0	1812.4	1578.9	1465.9	1407.7	1321.5	1286.8	186.9
540.0	1518.9	1346.9	1252.4	1205.2	1134.5	1104.4	186.9
660.0	1279.7	1139.6	1063.3	1024.6	964.9	940.8	186.9
780.0	1107.1	1001.8	933.1	902.6	850.5	831.3	186.9
900.0	953.1	876.4	821.4	794.2	746.5	728.6	186.9
1020.0	839.4	773.0	723.9	702.2	664.2	648.0	186.9
1140.0	749.3	691.0	649.4	631.2	598.4	585.0	186.9
1260.0	685.0	615.3	580.5	566.7	539.8	528.7	186.9
1380.0	633.7	567.7	535.3	523.2	498.3	488.9	186.9
1500.0	584.3	514.2	485.4	475.9	455.1	447.4	186.9
1620.0	541.6	471.3	446.7	438.6	420.4	414.2	186.9
1740.6	500.5	443.4	421.4	414.6	397.7	391.8	186.9
1860.0	427.4	377.2	361.3	357.6	346.1	342.7	186.9

TABLE 6A - CONTINUED

RUN NO. 3, CORE 1

INFINITE BOUNDARY CASE

TIME SEC.	LX1 PSQR	LX2 PSQR	LX3 PSQR	LX4 PSQR	LX5 PSQR	LX6 PSQR	LX7 PSQR
0.0	20922.9	20922.9	20922.9	20922.9	20922.9	20922.9	20922.9
1.8	20922.9	20922.9	20922.9	20922.9	20922.9	20922.9	186.3
3.6	20922.9	20922.9	20922.9	20922.9	20833.3	20669.1	186.3
5.4	20922.9	20922.9	20922.9	20922.9	20631.7	20348.3	186.3
7.2	20922.9	20870.6	20863.9	20787.7	20277.0	19894.4	186.3
9.0	20922.9	20861.9	20828.7	20697.3	19950.8	19512.6	186.3
10.8	20922.9	20694.9	20628.9	20443.1	19627.3	19134.4	186.3
12.6	20922.9	20607.6	20402.1	20262.2	19339.8	18825.9	186.3
14.4	20922.9	20505.8	20341.5	20061.7	19080.9	18519.8	186.3
16.2	20922.9	20380.3	20157.6	19818.3	18779.2	18216.2	186.3
18.0	20922.9	20239.8	19959.3	19588.1	18525.3	17948.0	186.3
19.8	20922.9	20104.3	19753.6	19350.9	18264.8	17701.6	186.3
21.6	20922.9	20007.7	19586.9	19159.4	18049.2	17489.4	186.3
FINITE BOUNDARY CASE							
21.6	20922.9	20007.7	19586.9	19159.4	18059.2	17489.4	186.3
40.0	20348.3	18440.1	17447.7	17008.7	15963.7	15437.4	186.3
53.0	19781.7	17473.0	16431.0	15881.9	14883.4	14382.6	186.3

TABLE 6A - CONTINUED

RUN NO. 4, CORE 1

CONSTANT EXTERNAL PRESSURE CASE

TIME SEC.	LX1 PSQR	LX2 PSQR	LX3 PSQR	LX4 PSQR	LX5 PSQR	LX6 PSQR	LX7 PSQR
0.0	31594.2	31594.2	31594.2	31594.2	31594.2	31594.2	31594.2
1.8	31594.2	31544.4	31544.4	31544.4	31505.4	31452.1	186.3
3.6	31594.2	31501.1	31501.1	31484.1	31250.3	31027.9	186.3
5.4	31594.2	31420.5	31379.8	31303.3	30799.4	30327.3	186.3
7.2	31594.2	31318.5	31229.1	31059.7	30289.0	29634.8	186.3
9.0	31594.2	31161.2	31047.7	30794.4	29814.1	29031.9	186.3
10.8	31594.2	30914.6	30801.5	30465.4	29339.4	28462.2	186.3
12.6	31594.2	30610.8	30498.3	30080.6	28871.9	27941.7	186.3
14.4	31594.2	30237.6	30125.7	29627.9	28354.3	27392.7	186.3
16.2	31594.2	30001.5	29890.1	29344.9	28018.6	27023.2	186.3
18.0	31594.2	29634.1	29523.3	28940.6	27601.7	26604.1	186.3
19.8	31594.2	29287.4	29177.2	28549.3	27197.8	26188.1	186.3
21.6	31594.2	28947.4	28837.9	28189.6	26839.4	25826.9	186.3
23.4	31594.2	28618.9	28510.2	27841.4	26499.8	26593.7	186.3
25.2	31594.2	28273.6	28165.4	27468.9	26136.4	25137.3	186.3
27.0	31594.2	27922.2	27814.7	27098.9	25775.5	24783.4	186.3
28.8	31594.2	27636.9	27529.9	26809.9	25483.7	24507.1	186.3
30.6	31594.2	27326.6	27220.2	26496.5	25188.1	24207.5	186.3

TABLE 6A - CONTINUED

RUN NO. 5, CORE 1

CONSTANT EXTERNAL PRESSURE CASE

TIME SECS.	LX1 PSQR	LX2 PSQR	LX3 PSQR	LX4 PSQR	LX5 PSQR	LX6 PSQR	LX7 PSQR
0	657.9	657.9	657.9	657.9	657.9	657.9	657.9
1.2	657.9	657.9	642.1	596.8	529.9	453.3	204.2
2.4	657.9	641.1	590.9	526.5	455.4	370.9	204.2
3.6	657.9	611.6	548.9	483.1	408.8	330.1	204.2
4.8	657.9	605.2	533.6	463.9	390.5	315.4	204.2
6.0	657.9	585.2	510.8	440.6	370.6	299.6	204.2

TABLE 7A
COMPUTER OUTPUT
EXPERIMENTAL BUILDUP

RUN NO. 6, CORE 2

CONSTANT INLET PRESSURE CASE

TIME SECS	LX1 PSQR	LX2 PSQR	LX3 PSQR	LX4 PSQR	LX5 PSQR	LX6 PSQR	LX7 PSQR
0	635.2	550.4	477.4	406.8	342.9	276.6	204.7
3	635.2	550.4	492.8	446.1	409.7	379.5	342.6
6	635.2	610.6	571.2	537.3	512.1	487.9	462.7
9	635.2	626.0	597.3	574.1	557.4	541.0	528.7
12	635.2	635.0	615.5	600.3	589.5	576.5	560.0
15	635.2	635.1	613.6	604.0	597.5	589.5	574.0
18	635.2	635.2	625.8	619.7	614.1	607.5	610.2

RUN NO. 7

0	956.8	824.8	700.7	581.8	467.4	359.9	240.6
3	956.8	864.9	772.8	701.2	644.1	596.8	590.4
6	956.8	907.0	860.2	776.7	781.2	741.2	710.2
9	956.8	956.6	919.8	893.6	873.8	854.8	840.3
12	956.8	956.7	943.5	928.5	914.8	898.2	897.6
15	956.8	956.7	947.5	936.5	924.6	912.7	908.1
18	956.8	956.7	950.8	942.1	933.1	924.8	923.5
21	956.8	956.7	952.8	946.4	940.6	933.6	930.6
24	956.8	956.7	956.6	953.4	944.9	944.2	943.5

TABLE 7A - CONTINUED

RUN NO. 8, CORE 1

CONSTANT INLET PRESSURE CASE

TIME SECS	LX1 PSQR	LX2 PSQR	LX3 PSQR	LX4 PSQR	LX5 PSQR	LX6 PSQR	LX7 PSQR
0	5695.5	2457.9	1864.8	1854.4	1738.8	1686.6	186.8
30.0	5695.5	2680.0	2058.9	1879.9	1767.3	1719.7	277.8
60.0	5694.5	2689.9	2073.8	1902.6	1817.3	1786.7	940.6
90.0	5695.5	2712.2	2108.2	1948.2	1880.9	1854.9	1250.9
120.0	5695.5	2757.5	2171.6	2022.2	1973.0	1959.7	1464.5
150.0	5695.5	2820.4	2249.3	2112.6	2078.3	2067.4	1645.8
180.0	5695.5	2883.0	2331.8	2194.8	2163.9	2155.6	1795.1
210.0	5695.5	2966.7	2429.8	2303.7	2274.2	2268.4	1942.1
240.0	5695.5	3048.1	2526.5	2407.4	2379.4	2376.4	2067.4
270.0	5695.5	3131.5	2630.7	2516.3	2489.9	2486.9	2177.9
300.0	5695.5	3202.4	2714.9	2605.9	2583.6	2583.6	2301.0
330.0	5695.5	3281.4	2812.1	2708.7	2690.4	2690.4	2417.6
360.0	5695.5	3350.9	2898.7	2798.6	2782.4	2782.4	2516.9
390.0	5695.5	3418.1	2981.2	2890.2	2876.0	2876.0	2628.0
420.0	5695.5	3504.9	3082.8	3000.7	2988.7	2988.7	2742.5
450.0	5695.5	3572.7	3169.6	3089.0	3076.8	3020.8	2848.2

TABLE 7A - CONTINUED

RUN NO. 9, CORE 1

NO INFLUX CASE

TIME SECS.	LX1 PSQR	LX2 PSQR	LX3 PSQR	LX4 PSQR	LX5 PSQR	LX6 PSQR	LX7 PSQR
0.0	5695.5	2655.3	2022.7	1835.2	1723.8	1671.9	186.8
30.0	4715.4	2601.5	2010.7	1831.9	1727.9	1678.4	584.0
60.0	3864.9	2464.4	1999.7	1850.4	1768.1	1737.9	940.6
90.0	3348.8	2323.6	1972.1	1858.7	1798.5	1778.2	1222.8
120.0	3021.6	2229.8	1964.5	1880.3	1838.6	1825.8	1418.9
150.0	2784.5	2174.8	1969.7	1910.5	1881.7	1873.9	1565.7
180.0	2618.2	2109.9	1954.4	1912.2	1893.0	1887.8	1653.9
210.0	2486.9	2072.5	1952.8	1925.3	1915.7	1915.7	1744.6
240.0	2368.7	2046.5	1953.9	1934.8	1927.1	1929.7	1812.1
270.0	2291.4	2034.7	1962.7	1952.1	1948.2	1950.9	1854.9
300.0	2215.5	2020.1	1968.8	1962.4	1962.4	1965.0	1889.5
330.0	2159.3	2010.5	1969.4	1969.5	1969.5	1972.1	1924.5
360.0	2122.3	2007.4	1976.6	1976.6	1976.6	1979.3	1942.1
390.0	2085.6	2003.6	1981.0	1981.0	1981.0	1986.4	1959.7
420.0	2067.4	2001.6	1981.0	1981.0	1981.0	1986.4	1977.5
450.0	2040.2	1994.8	1978.4	1978.4	1978.4	1986.4	1986.4

TABLE 8A
COMPUTER OUTPUT
NUMERICAL SOLUTIONS - INFINITE BOUNDARY, CORE 1

RUN NO. 1

TIME HOURS	LX1 PSQR	LX2 PSQR	LX3 PSQR	LX4 PSQR	LX5 PSQR	LX6 PSQR	LX7 PSQR
0.000	9930.7	9930.7	9930.7	9930.7	9930.7	9930.7	9930.7
0.0010	9930.7	9929.4	9927.1	9915.4	9859.5	9594.5	183.6
0.0020	9930.7	9919.9	9898.2	9817.6	9560.5	8871.5	183.6
0.0030	9930.7	9887.2	9824.2	9641.4	9222.8	8479.7	183.6
0.0040	9930.7	9815.2	9699.6	9424.3	8923.3	8155.7	183.6
0.0050	9930.7	9722.4	9570.7	9247.5	8713.3	7942.6	183.6
0.0060	9930.7	9571.1	9383.3	9014.7	8448.8	7676.9	183.6
0.0070	9930.7	9435.5	9232.1	8847.8	8274.4	7508.7	183.6
0.0080	9930.7	9286.8	9071.8	8678.2	8102.5	7345.5	183.6

TABLE 8A - CONTINUED

RUN NO. 2, CORE 1

TIME HOURS	LX1 PSQR	LX2 PSQR	LX3 PSQR	LX4 PSQR	LX5 PSQR	LX6 PSQR	LX7 PSQR
0.000	3121.5	3121.5	3121.5	3121.5	3121.5	3121.5	3121.5
0.0017	3121.5	3121.3	3120.7	3117.6	3102.2	3026.1	186.9
0.0033	3121.5	3119.9	3116.1	3100.5	3043.6	2869.5	186.9
0.0050	3121.5	3115.1	3103.6	3066.6	2966.9	2761.7	186.9
0.0067	3121.6	3104.4	3072.1	3022.4	2896.7	2678.7	186.9
0.0083	3121.5	3086.9	3053.8	2976.2	2834.7	2610.8	186.9
0.0100	3121.5	3063.3	3021.5	2931.1	2779.4	2552.9	186.9
0.0117	3121.5	3035.3	2986.9	2888.4	2729.4	2502.0	186.9
0.0134	3121.5	3004.4	2951.1	2846.3	2683.5	2456.4	186.9
0.0150	3121.5	2971.9	2914.9	2806.2	2640.8	2414.7	186.9
0.0167	3121.5	2938.7	2878.8	2767.4	2600.7	2376.0	186.9
0.0184	3121.5	2905.3	2843.0	2729.1	2562.7	2339.9	186.9

TABLE 8A - CONTINUED

RUN NO. 3, CORE 1

TIME HOURS	LX1 PSQR	LX2 PSQR	LX3 PSQR	LX4 PSQR	LX5 PSQR	LX6 PSQR	LX7 PSQR
0.000	20923.4	29823.4	20923.4	20923.4	20923.4	20923.4	20923.4
0.0005	20923.4	20923.1	20921.1	20908.2	20830.8	20372.8	186.3
0.0010	20923.4	20917.6	20898.9	20811.8	20455.4	19237.2	186.3
0.0015	20923.4	20893.7	20827.2	20588.8	19902.0	18401.3	186.3
0.0020	20923.4	20831.7	20686.8	20271.3	19355.2	17750.9	186.3
0.0025	20923.4	20739.1	20522.5	19985.7	18962.9	17337.3	186.3
0.0030	20923.4	20569.7	20266.7	19600.3	18470.6	16819.6	186.3
0.0035	20923.4	20397.9	20045.3	19316.9	18145.7	16495.9	186.3
0.0040	20923.4	20194.6	19802.7	19028.0	17829.7	16183.6	186.3
0.0045	20923.4	19967.9	19545.4	18738.2	17522.1	15884.9	186.3
0.0050	20923.4	19723.8	19279.2	18450.2	17225.1	15600.2	186.3
0.0055	20923.4	19471.6	19008.3	18165.9	16938.8	15329.2	186.3
0.0060	20923.4	19213.4	18736.3	17886.8	16662.8	15070.7	186.3
0.0065	20923.4	18944.1	18466.1	17613.6	16396.7	14823.7	186.3

TABLE 8A - CONTINUED

RUN NO. 4, CORE 1

TIME HOURS	LX1 PSQR	LX2 PSQR	LX3 PSQR	LX4 PSQR	LX5 PSQR	LX6 PSQR	LX7 PSQR
0.000	31594.3	31594.3	31594.3	31594.3	31594.3	31594.3	31594.3
0.0005	31594.3	31593.6	31588.1	31558.2	31403.1	30608.1	186.3
0.0010	31594.3	31576.6	31530.1	31339.4	30662.2	28635.3	186.3
0.0015	31594.3	31507.6	31354.1	30867.3	29639.6	27258.1	186.3
0.0020	31594.3	31341.9	31033.6	30243.9	28691.4	26201.7	186.3
0.0025	31594.3	31058.7	30601.0	29587.3	27862.3	25345.5	186.3
0.0030	31594.3	30745.9	30200.4	29080.5	27291.9	24785.5	186.3
0.0035	31594.3	30369.3	29757.2	28562.7	26733.0	24241.0	186.3
0.0040	31594.3	29823.7	29143.5	27877.5	26011.1	23542.6	186.3
0.0045	31594.3	29399.1	28692.8	27409.6	25544.4	23102.9	186.3

APPENDIX III

COMPUTER PROGRAMS

Nomenclature of the Computer Input and Output

A	-	Matrix
B	-	Elements of Matrix A
CF	-	Transducer calibration factor
CM	-	M_i as defined in equation (11)
D	-	Permeability
DP	-	Pressure difference between iterations, $psia^2$
DT	-	Time interval, hours
ERF	-	Error
FBP	-	Pressure at inlet, psia
KI	-	Iteration number
LX	-	Visicorder deflection (data from oscillograph)
MM	-	Run number
NV	-	Number of time intervals
PATM	-	Atmospheric pressure
PAV	-	Average pressure
PO	-	Initial inlet pressure
PSIA	-	Pressure in psia
PSQR	-	Pressure squared, $psia^2$
PSREF	-	Reference pressure
PTO	-	Outlet pressure
TINF	-	Transient time to reach inlet
U	-	Viscosity
YY	-	Y as defined in equation (10)
SOLUTN	-	Subroutine to solve Matrix A

FORTRAN SOURCE LIST

```
      SOURCE STATEMENT

C     COMPUTER PROGRAM - EXPERIMENTAL UNSTEADY STATE TESTS
$IBFTC DECKA   NODECK
      REAL LX(7,40)
      DIMENSION FBP(40),T(40),CF(5),PSIA(7,40),DP(7,40),PSQR(
     17,40),PTQR(7,40),PTO(40),PATM(7,40)
      READ(5,100)N,MMPSREF,ATM,PGS,DUMMY
  100 FORMAT (9X,213,4F10.2)
      READ(5,101)(FBP(I),I=1,N)
      READ(5,101)(PTO(I),I=1,N)
  101 FORMAT (6F10.1)
      READ (5,101)(T(J),J=1,N)
      READ (5,103)((LX(I,J),I=2,6),J=1,N)
  103 FORMAT (5F10.1)
      CF(1)=0.23
      CF(2)=0.24
      CF(3)=0.22
      CF(4)=0.30
      CF(5)=0.80
      DO 1 I=2,6
      DO 1 J=1,N
      LK=I-1
    1 DP(I,J)=LX(I,J)*CF(LK)
      PTM=(ATM/2.54)*0.491
      DO 2 J=1,N
    2 PSIA(1,J)=FBP(J)+PTM
      DO 9 J=1,N
    9 PSIA(7,J)=PTO(J)+PTM
      PREFA=PSREF+PTM
      DO 4 J=1,N
    4 PSIA(6,J)=PREFA+DP(6,J)
      DO 5 L=1,4
      I=6-L
      DO 5 J=1,N
      IL=I+1
    5 PSIA(I,J)=PSIA(IL,J)+DP(I,J)
      DO 6 I=1,7
      DO 6 J=1,N
    6 PSQR(I,J)=PSIA(I,J)*PSIA(I,J)
      DO 7 I=1,7
      DO 7 J=1,N
    7 PATM(I,J)=PSIA(I,J)/PTM
      DO 8 I=1,7
      DO 8 J=1,N
    8 PTQR(I,J)=PATM(I,J)*PATM(I,J)
      WRITE (6,104)MM
  104 FORMAT(1H1,32HEXPERIMENTAL RESULTS,    RUN NO.,I2,)
      IF (DUMMY.EQ.0.) GO TO 11
      WRITE (6,109)
  109 FORMAT (1HJ,3X,31HCONSTANT EXTERNAL PRESSURE CASE)
      GO TO 12
```

FORTRAN SOURCE LIST
(CONTINUED)

```
    SOURCE STATEMENT

 11 WRITE(6,105)
105 FORMAT(1HJ,3X,14HNO INFLUX CASE)
 12 WRITE(6,106)
106 FORMAT(1HJ,2X,4HTIME,10X,3HLX1,14X,3HLX2,14X,3HLX3,14X,3
   1HLX4,14X,3HLX5,14X,3HLX6,14X,3HLX7)
    WRITE (6,107)
107 FORMAT(1H ,11X,4HPSIA,4X,4HPSQR,5X,4HPSIA,4X,4
   1HPSQR,5X,4HPSIA,4X,4HPSQR,5X,4HPSIA,4X,4HPSQR,
   27X,4HPSIA,4X,4HPSQR,5X,4HPSIA,4X,4HPSQR,5X,4HPSIA,4X,4HPSQR)
    DO 10 J=1,N
 10 WRITE(6,108)T(J),(PSIA(I,J),PSQR(I,J),I=1,7)
108 FORMAT(1H ,F7.2,F9.2,F9.2,F8.2,F8.2,F9.2,F8.2,F9.2,
   1F8.2,F9.2,F8.2,F9.2,F8.2,F9.2)
    CALL EXIT
    STOP
    END
```

FORTRAN SOURCE LIST

SOURCE STATEMENT

```
C      COMPUTER PROGRAM - DRAWDOWN NUMERICAL CALCULATIONS
$IBFTC DECKA   NODECK
       COMMON Y(14),A(10,10),B(10),NV,YY(10),CM(14),TM(10)
       DIMENSION P(14),PP(14),DP(20)
       READ(5,100)NV,DT,POR,D1,D2,D3,X,PS,PA,PG,TINF
  100  FORMAT (7X,I3,6F10.4/4F10.4)
       PO=PA+PG
       Q=DT
       PAV=(PS+PO)/2.
       U=0.01772+0.0000017*PAV
       DO 1 J=1,7
     1 P(J)=PS
       DO 2 J=1,7
     2 Y(J)=P(J)*P(J)
       DO 3 J=1,5
       DO 3 I=1,5
     3 A(I,J)=0.0
       DO 4 I=1,4
       L=I+1
       A(L,I)=-D2
     4 A(I,L)=-D2
       DO 6 J=1,7
       UL=(7582.96*POR*U*X*X)/DT
     6 CM(J)=UL/P(J)
    11 CONTINUE
       B(1)=D1*(Y(1)-Y(2))+D2*(Y(3)-Y(2))+CM(2)*Y(2)+D1*Y(1)
       B(2)=D2*(Y(2)-Y(3))+D2*(Y(4)-Y(3))+CM(3)*Y(3)
       B(3)=D2*(Y(3)-Y(4))+D2*(Y(5)-Y(4))+CM(4)*Y(4)
       B(4)=D2*(Y(4)-Y(5))+D2*(Y(6)-Y(5))+CM(5)*Y(5)
       B(5)=D2*(Y(5)-Y(6))+D3*(Y(7)-Y(6))+CM(6)*Y(6)+D3*PO**2
       DO 7 KI=1,20
       A(1,1)=CM(2)+(D1+D2)
       A(2,2)=CM(3)+(2.*D2)
       A(3,3)=CM(4)+(2.*D2)
       A(4,4)=CM(5)+(2.*D2)
       A(5,5)=CM(6)+(D2+D3)
       CALL SOLUTN
       DP(KI)=YY(5)
       IF(KI.EQ.1) GO TO 201
       ERP=0.010*YY(5)
       IF(ABS(DP(KI)-DP(KI-1)).LE.ERP) GO TO 202
  201  DO 8 J=1,NV
       PP(J)=SQRT(YY(J))
     8 TM(J)=UL/PP(J)
       DO 9 I=2,6
       JI=I-1
     9 CM(I)=(TM(JI)-CM(I))/2.+CM(I)
       IF (KI.EQ.20) GO TO 202
     7 CONTINUE
  202  Y(7)=PO*PO
       WRITE (6,104)KI
```

FORTRAN SOURCE LIST
(CONTINUED)

```
    SOURCE STATEMENT

      WRITE(6,105)Q,P(1),Y(1),((PP(J),YY(J)),J=1,5),P(7),Y(7)
104   FORMAT (1H ,13HITERATION NO.,I3)
105   FORMAT(1HJ,F7.4,F9.2,F9.2,F8.2,F9.2,F8.2,F9.2,F8.2,F9.2,
     1F8.2,F9.2,F8.2,F9.2,F8.2,F9.2)
      Q=Q+DT
      DO 10 I=1,NV
      Y(I+1)=YY(I)
 10   P(I+1)=SQRT(Y(I+1))
      IF(Q.LT.TINF) GO TO 11
      CALL EXIT
      STOP
      END
```

FORTRAN SOURCE LIST

SOURCE STATEMENT

```
$IBFTC SOLUT   NODECK
       SUBROUTINE SOLUTN
       COMMON Y(14),A(10,10),B(10),NV,YY(10),CM(14),TM(10)
       DIMENSION AA(10,10),BB(10),AL(10,10),AM(10,10),AU(10,10)
      1,DIF(10),PCENT(10),AV(10,10)
  201 FORMAT(14X,14HSOLUTION ERROR/14X,6F15.6)
       M=NV
       DO 1 I=1,M
       DO 2 J=1,M
     2 AA(I,J)=A(I,J)
     1 BB(I)=B(I)
       CALCULATION OF L AND U
       DO 105 K=2,M
       KK=K-1
       DO 104 J=1,KK
       AL(J,K)=0.0
       AM(J,K)=0.0
       AU(K,J)=0.0
   104 AV(K,J)=0.0
   105 CONTINUE
       IF(A(1,1).EQ.0.) GO TO 150
   106 XIS=ABS(A(1,1))
       AL(1,1)=SQRT(XIS)
       AU(1,1)=A(1,1)/AL(1,1)
       DO 107 J=2,M
       AU(1,J)=A(1,J)/AL(1,1)
   107 AL(J,1)=A(J,1)/AU(1,1)
       DO 115 K=2,M
       KK=K-1
       VALUE=0.0
       DO 108 J=1,KK
   108 VALUE=VALUE+AL(K,J)*AU(J,K)
       ZX=A(K,K)-VALUE
       IF(ZX.EQ.0.) GO TO 150
   109 ZXX=ABS(ZX)
       AL(K,K)=SQRT(ZXX)
       AU(K,K)=ZX/AL(K,K)
       KP=K+1
       KK=K-1
       IF(KP.GT.M) GO TO 115
       DO 112 I=KP,M
       ZW=0.0
       ZV=0.0
       DO 110 LP=1,KK
       ZV=ZV+AL(K,LP)*AU(LP,I)
   110 ZW=ZW+AL(I,LP)*AU(LP,K)
       AU(K,I)=(A(K,I)-ZV)/AL(K,K)
   112 AL(I,K)=(A(I,K)-ZW)/AU(K,K)
   115 CONTINUE
       L AND U ARE CALCULATED
       PROCEEDING TO CALCULATE L-INVERSE AND U-INVERSE
```

FORTRAN SOURCE LIST
(CONTINUED)

```
    SOURCE STATEMENT

      DO 119 K=1,M
      AM(K,K)=1.0/AL(K,K)
  119 AV(K,K)=1.0/AU(K,K)
      DO 125 K=2,M
      KK=K-1
      DO 122 J=1,KK
      ZQ=0.0
      DO 120 L=J,KK
  120 ZQ=ZQ+AL(K,L)*AM(L,J)
  122 AM(K,J)=-ZQ/AL(K,K)
  125 CONTINUE
      IJN=M+1
      DO 135 KL=1,IJN
      K=IJN-KL
      IF(K.LE.1) GO TO 136
  126 DO 130 JK=1,K
      J=K-JK
      IF(J.LT.1) GO TO 135
  127 ZR=0.0
      JP=J+1
      DO 128 L=JP,K
  128 ZR=ZR+AU(J,L)*AV(L,K)
  130 AV(J,K)=-ZR/AU(J,J)
  135 CONTINUE
      PROCEEDING TO CALCULATE G-INVERSE=U-INVERSE*L-INVERSE
  136 DO 140 K=1,M
      DO 140 J=1,M
      A(J,K)=0.0
      DO 137 L=1,M
  137 A(J,K)=A(J,K)+AV(J,L)*AM(L,K)
  140 CONTINUE
      GO TO 152
  150 WRITE (6,151)
  151 FORMAT(1H ,29H THE METHOD IS NOT APPLICABLE)
  152 CONTINUE
      DO 153 I=1,M
      YY(I)=0.0
      DO 153 J=1,M
  153 YY(I)=YY(I)+A(I,J)*B(J)
  100 FORMAT(14X,5F15.6)
      WRITE (6,100)(YY(I),I=1,M)
      DO 9 J=1,M
      BOB=0.0
      DO 12 I=1,M
   12 BOB=BOB+AA(J,I)*YY(I)
      DIF(J)=BB(J)-BOB
      PCENT(J)=DIF(J)*100./BB(J)
    9 CONTINUE
      WRITE(6,201)(PCENT(J),J=1,M)
      YMAX=0.0
```

FORTRAN SOURCE LIST
(CONTINUED)

SOURCE STATEMENT

```
      DO 15 I=1,M
      IF (ABS(YY(I)).GT.YMAX) GO TO 16
      GO TO 15
   16 YMAX=ABS(YY(I))
   15 CONTINUE
      WRITE (6,100)YMAX
  202 DO 203 I=1,M
      DO 204 J=1,M
  204 A(I,J)=AA(I,J)
  203 B(I)=BB(I)
      RETURN
      END
```